Original Article

MOLECULAR METABOLISM

Increased α-HB links colorectal cancer and diabetes by potentiating NF-κB signaling

Xinyue Lv [1], Peipei Ding [1], Luying Li [1], Ling Li [1], Danlei Zhou [1], Xiaochao Wang [1], Jianfeng Chen [1], Wei Zhang [1], Qi Wang [1], Tian Liao [2], Wenyu Wen [1], Dawang Zhou [3], Qing-Hai Ji [2], Xianghuo He [1], Qun-Ying Lei [1], Weiguo Hu [1,*]

ABSTRACT

Sufficient evidence has linked many different types of cancers and T2D through shared risk factors; however, the underlying mechanisms are not fully understood. α-Hydroxybutyrate (α-HB), a byproduct metabolite increased in diabetes and cancer, including colorectal cancer (CRC), triggers lactate dehydrogenase A (LDHA) nuclear translocation. Nuclear LDHA markedly extends NF-κB nuclear retention by interacting with phosphorylated p65, leading to an increase in TNF-α production, impaired insulin secretion and the exacerbation of azoxymethane (AOM)/dextran sodium sulfate (DSS)-induced CRC and high-fat diet (HFD)-induced type 2 diabetes. Furthermore, metformin interrupted this process by inhibiting the transcription of FOXM1 and c-MYC, the resultant downregulation of LDHA expression and α-HB-induced LDHA nuclear translocation. Thus, the results reveal the elevated α-HB level could be a novel shared risk factor of linking CRC, diabetes and the use of metformin treatment, as well as highlight the importance of preventing NF-κB activation for protecting against cancer and diabetes.

Keywords α-Hydroxybutyrate; Type 2 diabetes; Colorectal cancer; Lactate dehydrogenase A; NF-κB

1. INTRODUCTION

Cancer is becoming a leading cause of death and the global cancer burden is still increasing [1]. Epidemiological studies have reported the increased risk of diabetes in adolescent and adult cancer survivors [2], while the increased risk of certain kinds of cancer, including colon, pancreas, bladder, breast, cervial, stomach and liver, has also been observed in patients with type 2 diabetes (T2D) [3], indicating the positive association between diabetes and cancers. The biological mechanisms underscoring the relationship between the two multifactorial disorders involve several common risk factors, including aging, sex, lifestyle factors, hyperglycemia and chronic inflammation [4], however, it still requires further exploration for the development of effective prophylactic and therapeutic strategies.

The overproduction of reactive oxygen species (ROS) and a variety of inflammatory mediators, such as TNF-α and IL-6[5,6], predisposing individuals to a systemic, chronic, and low-grade metabolic inflammatory state (termed metaflammation) and resultant immunological disorders, largely contributing to the development of various diseases, including cancers and T2D [7]. Many cancers develop from infectious and chronic inflammatory sites, and an inflammatory condition often precedes the development of cancer. Proinflammatory transcription factors such as NF-κB and STAT3 are constitutively activated in various cancer types; thus, inflammation is a critical component of carcinogenesis and tumor progression [8]. In addition, diabetes is usually associated with a low-grade proinflammatory state [9]. Thus, metaflammation appears to be a key connection between cancer and T2D.

Cancer and diabetes are common metabolic disorders, charaterized by extensive changes in various metabolites, such as amino acids and their derivatives [10], lipid metabolites [11] and carbohydrates [12], but the functions of these factors in diseases-associated complications remain largely unknown. α-Hydroxybutyrate (α-HB) is an organic acid catalyzed by lactate dehydrogenase (LDH) from α-ketobutyrate (α-KB) and is involved in threonine and methionine—cysteine metabolism and glutathione synthesis [13]. Increased cysteine levels have been observed in patients with cancer and diabetes, which may lead to elevated α-KB and α-HB levels, while methionine restriction in the diet can suppress tumorigenesis and improve insulin sensitivity [14—17]. To identify metabolite biomarkers for cancer diagnosis, increased α-HB levels have been observed in certain types of cancer, such as colorectal cancer (CRC) [18,19], hepatocellular carcinoma [20], gastric cancer [21], lung cancer [22] and diffuse large B-cell lymphoma [23]. In addition, consistent with upregulated cysteine levels, increased α-HB concentrations in the plasma of diabetic patients predict insulin resistance and impaired glucose homeostasis [13], which was further verified by accumulating evidence [24—26]. The decline in α-HB induced by gastric bypass surgery significantly improves insulin sensitivity in patients, further suggesting that α-HB is a potential biomarker for tracking glycemic conditions and detecting impaired

[1]Fudan University Shanghai Cancer Center and Institutes of Biomedical Sciences, Shanghai Medical College, Fudan University, Shanghai, 200032, China [2]State Key Laboratory of Cellular Stress Biology, Innovation Center for Cell Signaling Network, School of Life Sciences, Xiamen University, Xiamen, Fujian, 361102, China [3]Key Laboratory of Breast Cancer in Shanghai, Fudan University Shanghai Cancer Center, Fudan University, Shanghai, 200032, China

*Corresponding author. E-mail: weiguohu@fudan.edu.cn (W. Hu).

Received January 29, 2023 • Revision received May 31, 2023 • Accepted June 28, 2023 • Available online 4 July 2023

https://doi.org/10.1016/j.molmet.2023.101766

glucose homeostasis [27]. Moreover, the relationship between upregulated α-HB and other diseases, including obesity [28,29], remote ischemic conditions [30] and metabolic syndrome [31], has also been disclosed.

The role of inflammation in T2D and certain cancers has been highly examined; however, it is unclear whether or how α-HB is linked to metainflammation in these human disorders. Here, we investigated the biological function and regulatory mechanism by which α-HB links CRC and T2D.

2. RESULTS

2.1. α-HB treatment exacerbates AOM/DSS-induced CRC in mice

Given the upregulation of α-HB in CRC patients [18], we first explored whether α-HB treatment could affect AOM/DSS-induced CRC, a conventional inflammation-driven murine CRC model [32,33]. The results showed that combined α-HB treatment significantly increased tumor volumes and diameters in colorectal sites and mortality rate, while decreased overall surivival compared to AOM/DSS alone (Figure 1A,B, Figs. S1A and S1B), suggesting a protumorigenic effect of α-HB on inflammation-driven CRC development. In addition, AOM/DSS alone resulted in significant body weight loss and shorter colon lengths compared to the control treatment, while the combination with α-HB further worsened these conditions. However, α-HB alone had no effect on body weight or colon length, similar to the control treatment (Figure 1C,D). These results indicate that α-HB may exacerbate AOM/DSS-induced local inflammatory injury and subsequent CRC development, while α-HB alone had no effect on initiating inflammatory injury.

The crosstalk between the immune system and tumors plays an important role in cancer pathogenesis, including inflammation-driven CRC tumorigenesis [33]. Next, we performed flow cytometry to examine immune cells, including $CD4^+$ and $CD8^+$ T cells, B cells, macrophages, myeloid-derived suppressor cells (MDSCs), neutrophils, NK cells, NKT cells, DCs and/or Ter cells, in the spleen, blood and/or colon. Compared to control treatment, α-HB alone did not affect the proportions of these immune cells in any of the three locations except for reducing NK cells in the spleen (Fig. S1C) and B cells in blood (Fig. S1M), and elevating NKT, MDSCs in blood (Fig. S1O), while AOM/DSS alone reduced NK cells in the spleen (Fig. S1C), $CD4^+$ and $CD8^+$ T cells and B cells in blood (Fig. S1K-M) and elevated MDSCs in the colon (Figure 1G) and blood (Fig. S1O), neutrophils in blood (Fig. S1P), and macrophages and neutrophils in the colon (Fig. S1S-T). Furthermore, compared to AOM/DSS treatment alone, combined α-HB treatment reduced $CD4^+$ and $CD8^+$ T cells and NK cells in the spleen (Figure 1E,F, and Fig. S1C) and increased MDSCs in the colon (Figure 1G) and Ter cells in the spleen (Fig. S1D). Ter cells are tumor-inducible, erythroblast-like cells deriving from megakaryocyte-erythroid progenitor cells, promoting tumor progression by secreting neurotrophic factor artemin [34]. Besides, using an immunohistochemical assay, we further confirmed the significantly reduced levels of $CD4^+$ and $CD8^+$ T cells in the colon in response to α-HB combined treatment compared to AOM/DSS alone (Fig. S1U). Next, we measured the levels of 39 cytokines and chemokines in colon tissue homogenates (CTHs) using LEGENDplex Multiplex Bead Assays. Consistent with the results in immune cells, α-HB alone failed to markedly alter the expression of 39 cytokines and chemokines compared to the control treatment (Fig. S2). Of the 39 cytokines and chemokines, TNF-α was increased dramatically in the colon in mice after α-HB combined treatment compared to the effect of AOM/DSS alone, although AOM/DSS alone did significantly upregulate TNF-α levels (Figure 1H). In addition, we found that in the AOM/DSS treatment groups, combined α-HB increased local IL-6 levels without a significant difference (Figure 1I) and reduced local CXCL13 levels with a slight difference (Fig. S2Ba). These results support our and other findings that the reverse correlation between $CD8^+$ T cells and the MDSC proportion is closely associated with CRC tumorigenesis [33], and TNF-α and IL-6 are highly involved in the development of colitis-associated cancer [35,36]. The increased local TNF-α level may facilitate the survival, recruitment and function of MDSCs that impair the antitumor immune response of $CD8^+$ T cells [37]. Furthermore, TNF-α may directly stimulate activation-induced cell death in T cells, especially $CD8^+$ T cells [38]. The lower CXCL13 level in the α-HB combination group suggests that fewer $CXCR5^+$ B or T cells were recruited to the local inflammatory microenvironment than in the AOM/DSS alone group [39,40].

Next, we measured the plasma α-HB concentration to quantitatively decipher its association with tumor development and the immune response. It has been recognized that ROS can accumulate in the local CRC site [41], thus increasing α-HB production [42]. We observed a significant increase in the plasma α-HB concentration after α-HB or AOM/DSS administration, and combined treatment with AOM/DSS and α-HB further elevated plasma α-HB levels (Figure 1J). Furthermore, the plasma α-HB concentration was closely correlated with tumor size (Figure 1K) and number (Figure 1L), local levels of TNF-α (Figure 1M) and IL-6 (Figure 1N), $CD4^+$ (Figure 1O) and $CD8^+$ (Figure 1P) T cells in the spleen, and MDSCs in the colon (Figure 1Q). Taken together, these findings suggest that α-HB can accelerate the progression of inflammation-driven CRC in an AOM/DSS-induced murine model by potentiating inflammation and impairing antitumor immunity, and this effect may be mediated by increased local TNF-α.

2.2. α-HB promotes insulin resistance in HFD-induced obesity-associated murine T2D

Due to the tight link between cancer and insulin resistance/T2D, we next investigated the role of α-HB in high-fat diet (HFD)-induced T2D. After treatment with normal chow (NC, and no α-HB), α-HB, HFD, or α-HB plus HFD for 24 weeks, the body weight in both HFD-fed groups increased as expected, while α-HB failed to induce any alterations regardless of HFD or normal chow feeding (Fig. S3A), indicating that a HFD but not α-HB affects body weight. To further explore the effect of α-HB on glucose homeostasis, we performed the glucose tolerance test (GTT) and insulin tolerance test (ITT) on all four groups of mice. Consistent with the body weight change, α-HB alone induced the same effect as NC on the GTT (Figure 2A) and ITT (Figure 2B). However, mice fed a HFD alone showed much more intolerance to glucose and insulin than mice that received NC and α-HB alone, which was further worsened by the additional α-HB treatment (Figure 2A,B). This result suggests that α-HB alone has no effect on glucose homeostasis, but it can exacerbate HFD-induced obesity-associated insulin resistance as a concurrent treatment.

Accumulating evidence demonstrates that activation of the immune system and cytokine-mediated chronic inflammation are highly involved in the pathogenesis of T2D [43]. To investigate possible immune system changes in the different groups, we analyzed the proportions of $CD4^+$ and $CD8^+$ T cells, macrophages and neutrophils in the spleen, blood, and two central organs involved in glucose and lipid metabolism (the liver and epididymal adipose tissue) by flow cytometry. Consistent with the effect on glucose homeostasis, α-HB had no effect on the composition of immune cells in these tissues in NC-fed mice (Figure 2C, Fig. S3B-Q). Furthermore, a HFD also induced

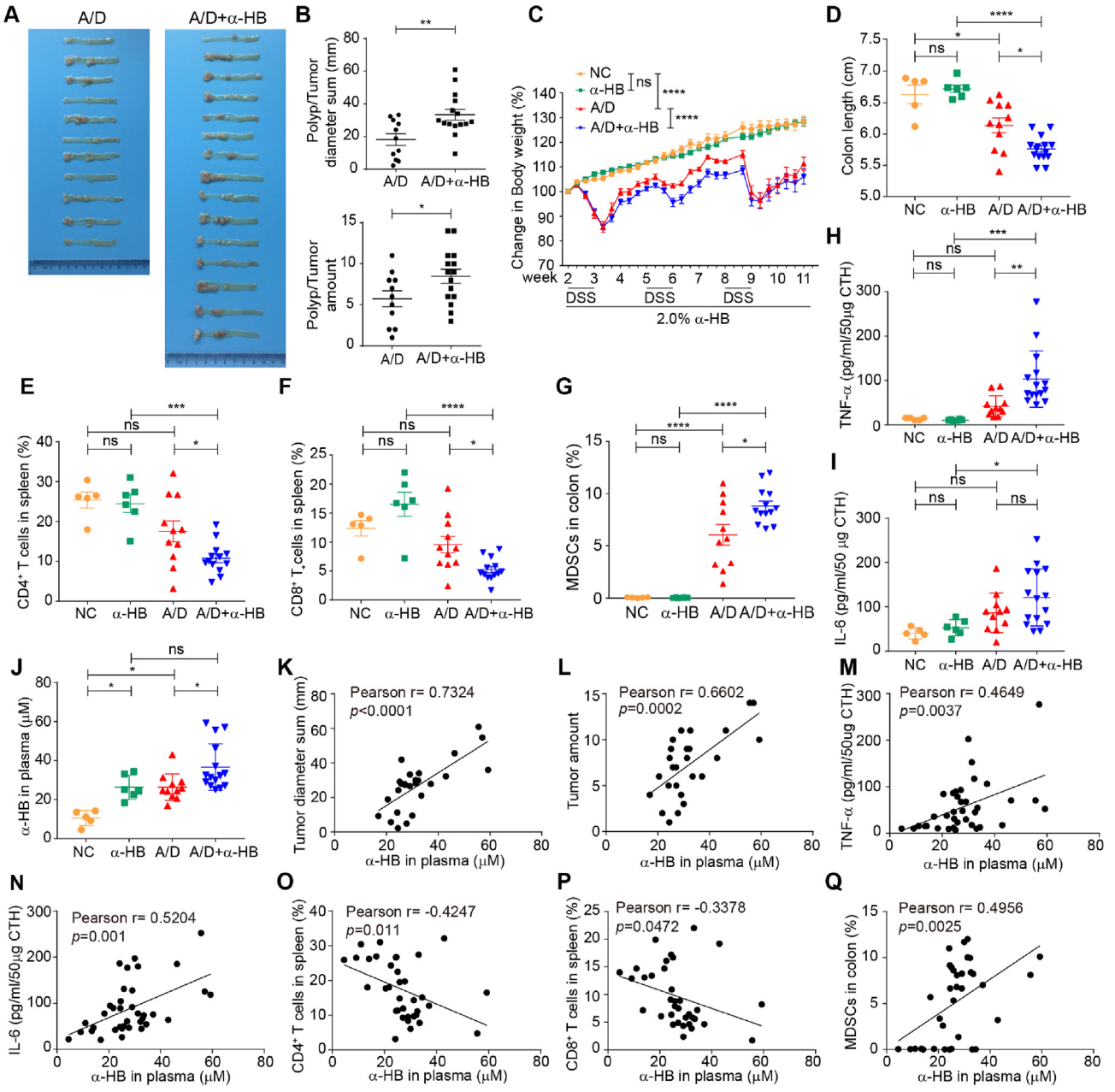

Figure 1: α-HB treatment promotes AOM/DSS-induced CRC. (A) Images of colons in the A/D and A/D+α-HB groups collected at the end of the CRC induction regimen. (B) Polyp/Tumor diameter sums and numbers were measured and counted in the A/D and A/D+α-HB groups. (C–D) Body weights changes and colon lengths in the four groups were calculated. (E–G) $CD4^+$ T cells (E, defined as $CD3^+$ and $CD4^+$) and $CD8^+$ T cells (F, defined as $CD3^+$ and $CD8^+$) in the spleen and MDSCs (G, defined as $CD11b^+$ and $Gr\text{-}1^+$) in colon were examined by flow cytometry. (H–I) Local concentrations of TNF-α (H) and IL-6 (I) in CTH of the four groups were measured by ELISA. (J) α-HB concentrations in the plasma in the NC, α-HB, A/D and A/D+α-HB groups were determined by LC/MS–MS. (K–Q) The correlation between α-HB concentrations and tumor diameter sums (K), tumor numbers (L), TNF-α (M) and IL-6 (N) concentrations in CTH, $CD4^+$ T cells (O) and $CD8^+$ T cells (P) in the spleen and MDSCs (Q) in the colon. NC, n = 5; α-HB, n = 6; A/D, n = 11; A/D+α-HB, n = 15 (A-D, O-Q). NC, n = 5; α-HB, n = 6; A/D, n = 11; A/D+α-HB, n = 13 (H-L, M–N). The data are shown as the mean ± SEM; NC, negative control. A/D, AOM/DSS. CTH, colonic tissue homogenate. NS, not significant; Statistical differences were determined by two-tailed unpaired Student's *t*-tests (B), two-way ANOVA test (C) and one-way ANOVA test (D–J) with Tukey's multiple comparison. The *p* values were considered significant if < 0.05. *, **, *** and **** denote $p < 0.05$, $p < 0.01$, $p < 0.005$ and $p < 0.001$, respectively.

similar results, except for significantly increasing the proportions of all four immune cell types only in adipose tissue (Fig. S3N-Q) but not in blood, spleen or liver (Fig. S3B-M). In addition, concurrent treatment with α-HB failed to alter the effect of HFD on any of these immune cells in the four tissues (Fig. S3B-Q). Adipose tissue macrophages contribute to local inflammation and insulin resistance via polarization, and M1 macrophages induce insulin resistance by producing inflammatory mediators, such as TNF-α, IL-6, and nitric oxide, while M2 macrophages maintain insulin sensitivity via anti-inflammatory mediators such as IL-10 [44]. We observed that a HFD significantly increased M1 cells (Figure 2C) while reducing M2 (Figure 2D) macrophages in both the liver and adipose tissue. However, the combined

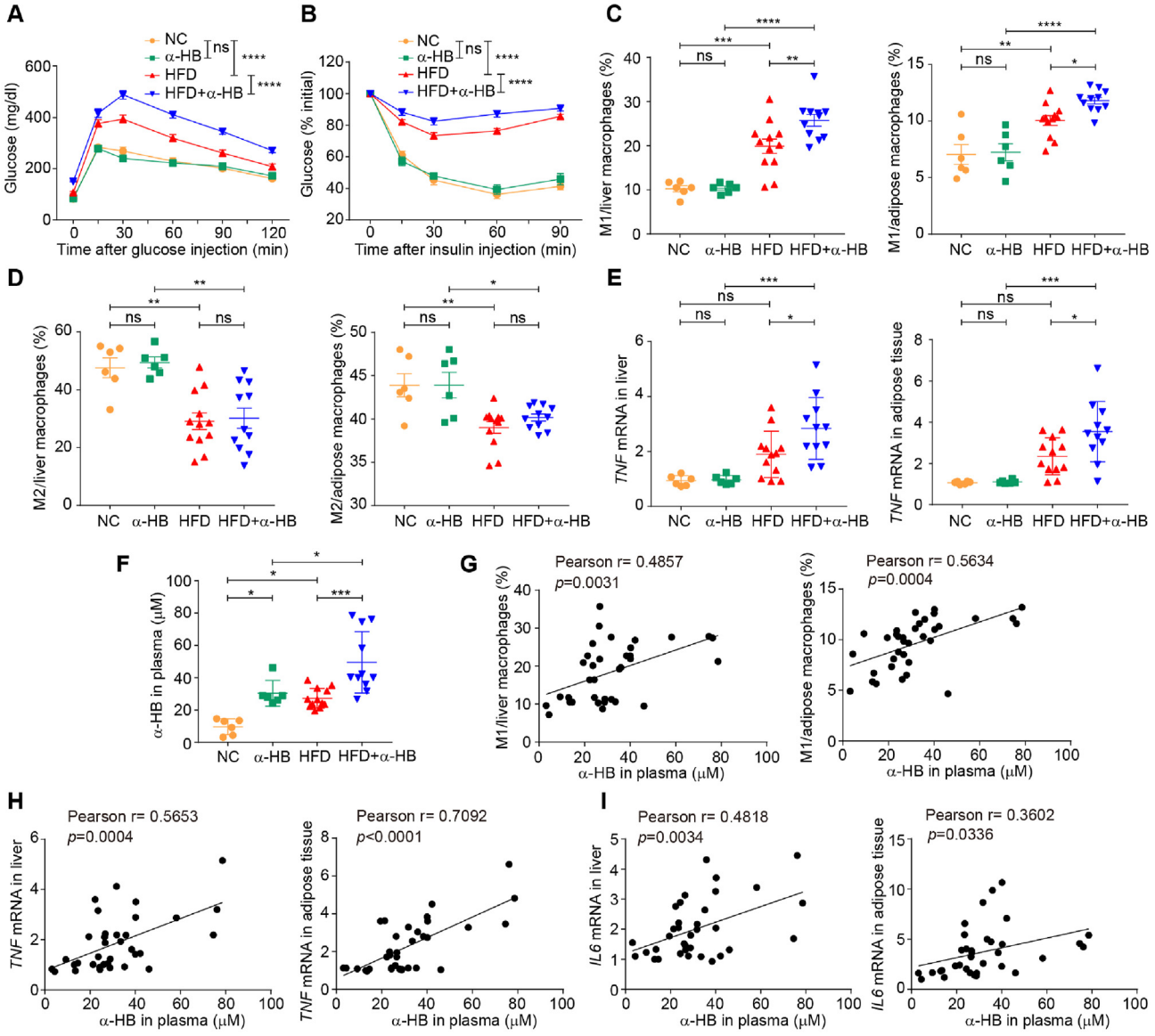

Figure 2: α-HB administration accelerates HFD-induced type 2 diabetes. (A) Blood glucose concentrations of the four groups, as measured by the GTT. (B) Blood glucose as a percentage of the basal value in the four groups, as measured by the ITT. (C—D) M1 macrophages (defined as $CD45^+F4/80^+CD11c^+$, C) and M2 macrophages (defined as $CD45^+F4/80^+CD206^+$, D) in liver (left) and adipose tissue (right) were determined by flow cytometry. (E) *TNF* levels in liver (left) and adipose tissue (right) were determined by RT-PCR. (F) Plasma α-HB concentrations in the NC, α-HB, HFD and HFD+α-HB groups were determined by LC/MS—MS. (G—I) The correlation between α-HB concentrations and M1 macrophages (G), *TNF* (H) and *IL6* (I) in liver and adipose tissue. NC, n = 6; α-HB, n = 6; HFD, n = 12; HFD+α-HB, n = 11 (C-D, G). The data are shown as the mean ± SEM; NC, negative control; HFD, high-fat diet; GTT, glucose tolerance test; ITT, insulin tolerance test; LC/MS—MS, liquid chromatography mass spectrometry; NS, not significant; Statistical differences were determined by two-way ANOVA test (A—B) and one-way ANOVA test (C—F). The *p* values were considered significant if < 0.05. *, **, *** and **** denote $p < 0.05$, $p < 0.01$, $p < 0.005$ and $p < 0.001$, respectively.

α-HB treatment further increased M1 macrophages (Figure 2C) but had no effect on M2 macrophages (Figure 2D) in either the liver or adipose tissues, suggesting that the exacerbated insulin resistance induced by α-HB may be mediated by the increased number of M1 macrophages in liver and adipose tissues.

Given the association between cytokines/chemokines and the inflammatory state in diabetes, we further examined alterations in cytokines/chemokines in liver and adipose tissues by qRT-PCR. Compared to NC, α-HB treatment alone had no effect on the expression of the tested cytokines/chemokines (Figure 2E, and Fig. S4), while a HFD strongly elevated the expression levels of TNF-α (Figure 2E) and IL-6 (Figs. S4A and F) in both liver and adipose tissues, accompanied by increased IL-12 (Fig. S4I) and reduced CXCL9 (Fig. S4Q) in adipose tissues. Furthermore, the combined treatment of α-HB with a HFD significantly increased TNF-α (Figure 2E) and IL-6, although without statistical significance (Figs. S4A and F), in both liver and adipose tissues. We also found that α-HB treatment reduced IL-10 in the liver (Fig. S4B) but not adipose tissues (Fig. S4G) compared to the effect of a HFD. Both TNF-α and IL-6 are markers of M1 macrophages and central mediators of inflammatory responses, while IL-10 is a marker of M2 macrophages and a classic anti-inflammatory cytokine; thus, these

results further support the role of inflammation in glucose homeostasis [44].

We next analyzed the association between the immune response and α-HB by measuring plasma α-HB concentrations. HFD significantly elevated the plasma α-HB concentration to a level comparable with that induced by α-HB alone, while their combination potently increased the plasma α-HB concentration further (Figure 2F). Based on these results, we found that M1 polarization (Figure 2G) and the expression levels of TNF-α (Figure 2H) and IL-6 (Figure 2I) in the liver and adipose tissues in the four groups of mice were closely correlated with the plasma α-HB concentration. Taken together, these results indicate that α-HB could worsen HFD-induced obesity-associated murine T2D due to the exacerbated inflammatory state mediated by increased M1 macrophage polarization, the elevated levels of TNF-α and IL-6 and the reduced levels of IL-10 in liver and adipose tissues.

2.3. α-HB potentiates NF-κB activation

The local level of TNF-α was significantly elevated by the combined treatment of α-HB and AOM/DSS or HFD but not by α-HB alone in CRC and T2D murine models, and IL-6 also displayed a similar trend, although without statistical significance. Considering the key role of NF-κB in the transcriptional regulation of TNF-α and IL-6, thus linking inflammation, cancer [8,36] and T2D [45,46], we hypothesized that the presence of the NF-κB activator α-HB may further augment NF-κB activation. Lipopolysaccharide (LPS), a common NF-κB activator, has been reported to be elevated in these two diseases [45,47]. Thus, we explored the effect of α-HB on LPS-induced NF-κB activation in human colorectal epithelial SW620 cells, murine insulinoma MIN6 cells, which has the characteristics of pancreatic beta cells, and murine pre-adipocytes 3T3-L1 cells.

Upon LPS stimulation, NF-κB activation, as indicated by increased p65 (S536) phosphorylation (Figure 3A and Fig. S5A) and nuclear p65/p50 accumulation (Fig. S6A), was visibly prolonged by concurrent α-HB treatment in SW620, MIN6 and 3T3-L1 cells. At a certain concentration of LPS (Figure 3B, Fig. S5B and Fig. S6B) or α-HB (Figure 3C, Fig. S5C and Fig. S6C), the phosphorylation and nuclear accumulation of NF-κB were also enhanced in a dose-dependent manner. We further observed a similar effect of α-HB on NF-κB activation in the above murine

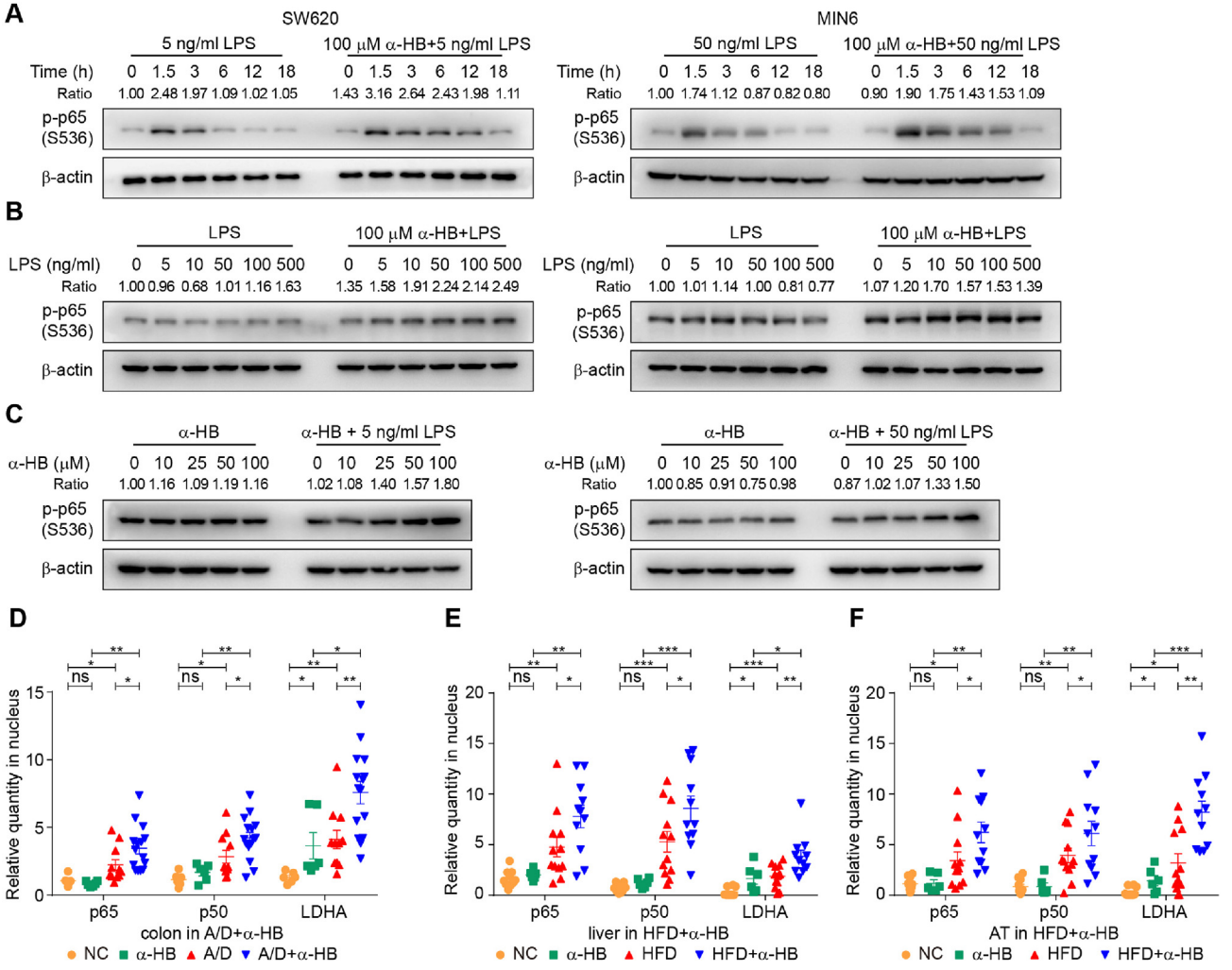

Figure 3: α-HB enhances LPS-induced NF-κB activity. (A–C) The 48 h-preincubation of α-HB prolonged the p65 S536 phosphorylation levels in SW620 (left) and MIN6 (right) cells in a time-dependent (A), LPS-dependent (B) and α-HB-dependent manner (C). Samples were collected 6 h after LPS stimulation in Figure B and C. (D–F) Quantification of p65, p50 and LDHA levels in nuclear extracts of colon tissue in the A/D+α-HB model (D) and liver (E) and adipose tissue (F) in the HFD+α-HB model. Histone H3 was used as a loading control for immunoblotting. The data are shown as the mean ± SEM; NC, negative control; NS, not significant; Statistical differences were determined by one-way ANOVA test with Tukey's multiple comparison. The p values were considered significant if < 0.05. *, ** and *** denote $p < 0.05$, $p < 0.01$ and $p < 0.005$, respectively.

models, which was determined by examining nuclear accumulation by immunoblotting in colorectal sites of the AOM/DSS-induced CRC model, AOM/DSS alone but not α-HB alone significantly increased p65/p50 nuclear accumulation, which was further enhanced by combined treatment with α-HB (Figure 3D and Fig. S6D). Similar results were observed in the liver and adipose tissue of the HFD-induced T2D model. HFD alone but not α-HB alone obviously promoted p65/p50 nuclear accumulation, and this effect was further enhanced by concurrent treatment with α-HB (Figure 3E,F, and Figs. S6E and F).

Next, we explored the functional effect of α-HB on NF-κB activation by measuring the level of its classic downstream target TNF-α. At the transcriptional level, concurrent α-HB treatment further significantly enhanced *TNF* expression in a time-dependent (Figure 4A and Fig. S5D) and dose-dependent (Figure 4B and Fig. S5E) manner after LPS stimulation. At the translational level, we observed similar results. As shown in Figure 4C, the level of TNF-α in the supernatant of SW620 cells increased gradually with increasing LPS concentrations, and this effect was enhanced by concurrent α-HB treatment. Furthermore, increasing concentrations of α-HB elevated supernatant TNF-α levels in SW620 cells in a dose-dependent manner after LPS stimulation (Figure 4D). In addition, NF-κB activation is related to pancreatic β cell apoptosis and dysfunction [48]; thus, we measured the supernatant insulin levels in MIN6 cells after LPS and/or α-HB treatment. We observed that only high glucose stimulation along with α-HB and/or LPS induced impact on insulin secretion. LPS alone but not α-HB alone significantly reduced insulin production, while the combined treatment markedly reduced insulin concentrations; however, this effect was significantly abrogated by the NF-κB inhibitor PDTC (Figure 4E,F). This

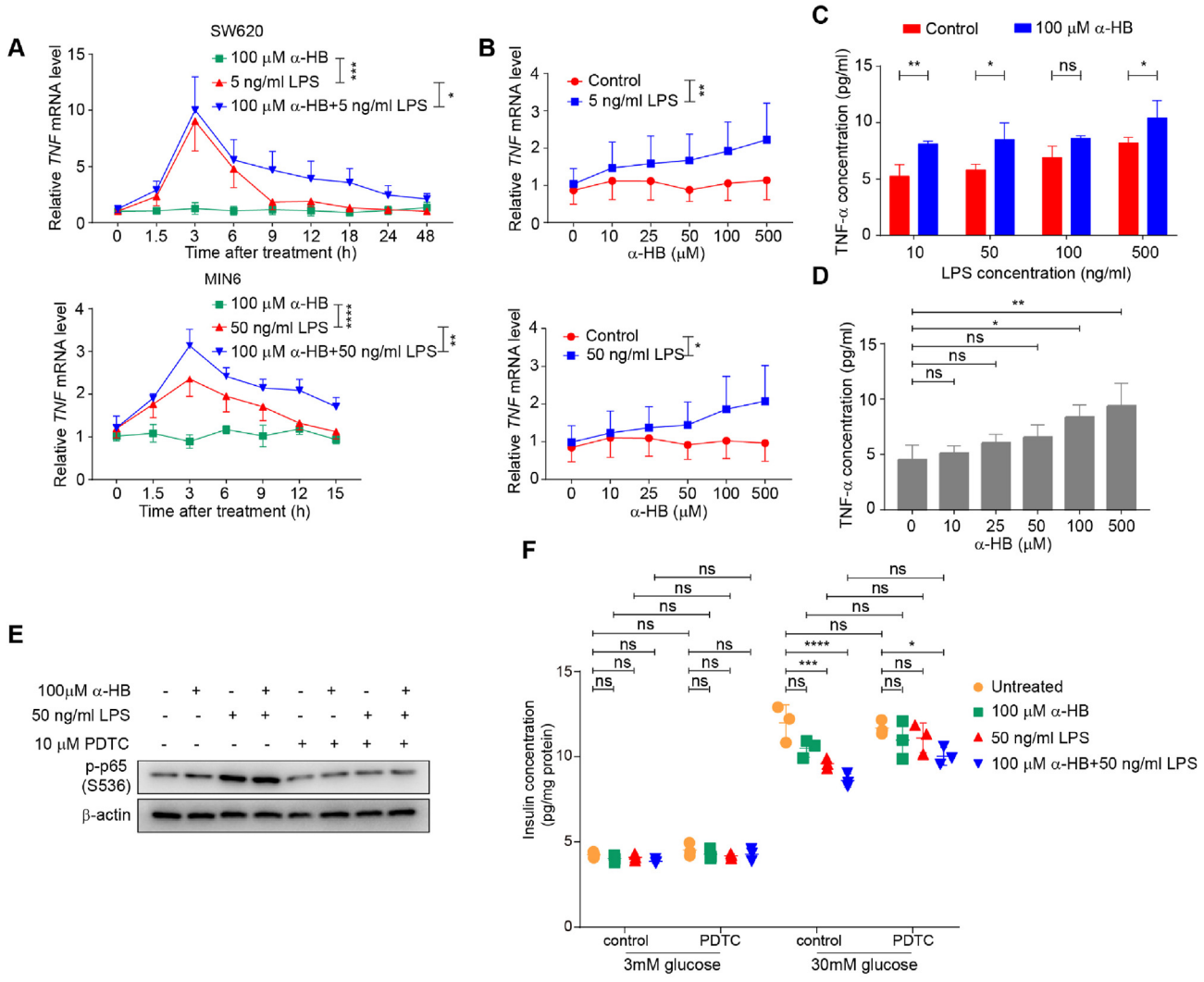

Figure 4: α-HB enhances LPS-induced NF-κB functions. (A) *TNF* levels in SW620 (upper) and MIN6 (bottom) cells treated with α-HB and/or LPS for different times were determined by qRT-PCR. (B) *TNF* levels in SW620 (upper) and MIN6 (bottom) cells treated with different concentrations of α-HB and/or LPS for 9 h were determined by qRT-PCR. (C) TNF-α concentrations in the supernatant of SW620 cells treated with LPS for 60 h with or without α-HB was determined by ELISA. (D) TNF-α concentrations in the supernatant of SW620 cells treated with LPS and different concentrations of α-HB for 60 h was determined by ELISA. (E) The inhibitory effect of 12 h preincubation of PDTC on LPS-induced NF-κB activity in MIN6 cells. (F) GSIS was measured by ELISA in MIN6 cells treated with α-HB and/or LPS in the presence or absence of PDTC. The data are shown as the mean ± SD; NC, negative control; GSIS, glucose-stimulated insulin secretion; NS, not significant; Statistical differences were determined by two-way ANOVA test (A–C), one-way ANOVA test (D) and three-way ANOVA test (F) with Tukey's or Sidak's multiple comparison test. The *p* values were considered significant if < 0.05. *, **, *** and **** denote $p < 0.05$, $p < 0.01$, $p < 0.005$ and $p < 0.001$, respectively.

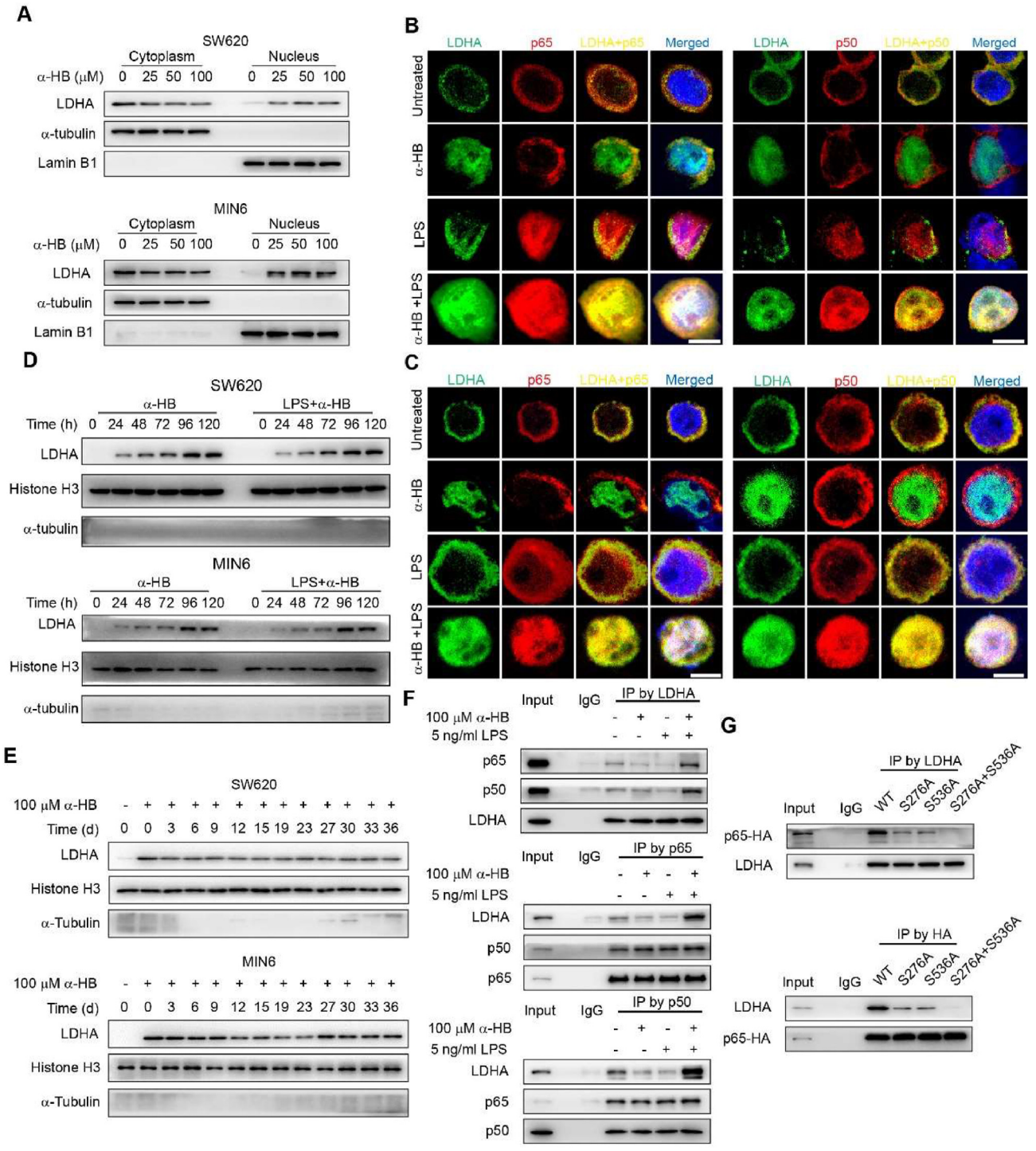

Figure 5: α-HB-induced LDHA nuclear translocation extends NF-κB nuclear retention. (A) Cellular distribution of LDHA in SW620 (upper) and MIN6 (bottom) cells treated with different concentrations of α-HB for 48 h. (B–C) ICC images of LDHA (green), p65 (red, upper) and p50 (red, bottom) in SW620 cells after 48 h-preincubation of α-HB and/or LPS treatment for 1.5 h (B) and 12 h (C), as indicated by DAPI (blue). Scale bars, 7.5 μm. (D) Nuclear LDHA accumulation over time in SW620 and MIN6 cells with continuous α-HB and/or LPS treatment. (E) The time course of LDHA nuclear retention in SW620 and MIN6 cells after 48 h of α-HB treatment. (F) Immunoprecipitation analysis of the interactions among LDHA (upper), p65 (middle) and p50 (bottom) in SW620 cells treated with α-HB for 48 h and/or LPS for 1.5 h. (G) The effects of p65 phosphorylation sites on the interaction between LDHA and p65 were detected in p65 WT/mutant plasmids tranfected-SW620 cells treated with a 48 h-preincubated α-HB treatment and/or LPS stimulation for 1.5 h.

result further supports α-HB as an independent predictor of worsening glucose tolerance; more importantly, NF-κB inhibition may hold potential prophylactic and therapeutic use for T2D. Taken together, these results suggested that α-HB could considerably prolong LPS-induced NF-κB nuclear retention, thus upregulating and maintaining TNF-α expression and impairing glucose-induced insulin secretion.

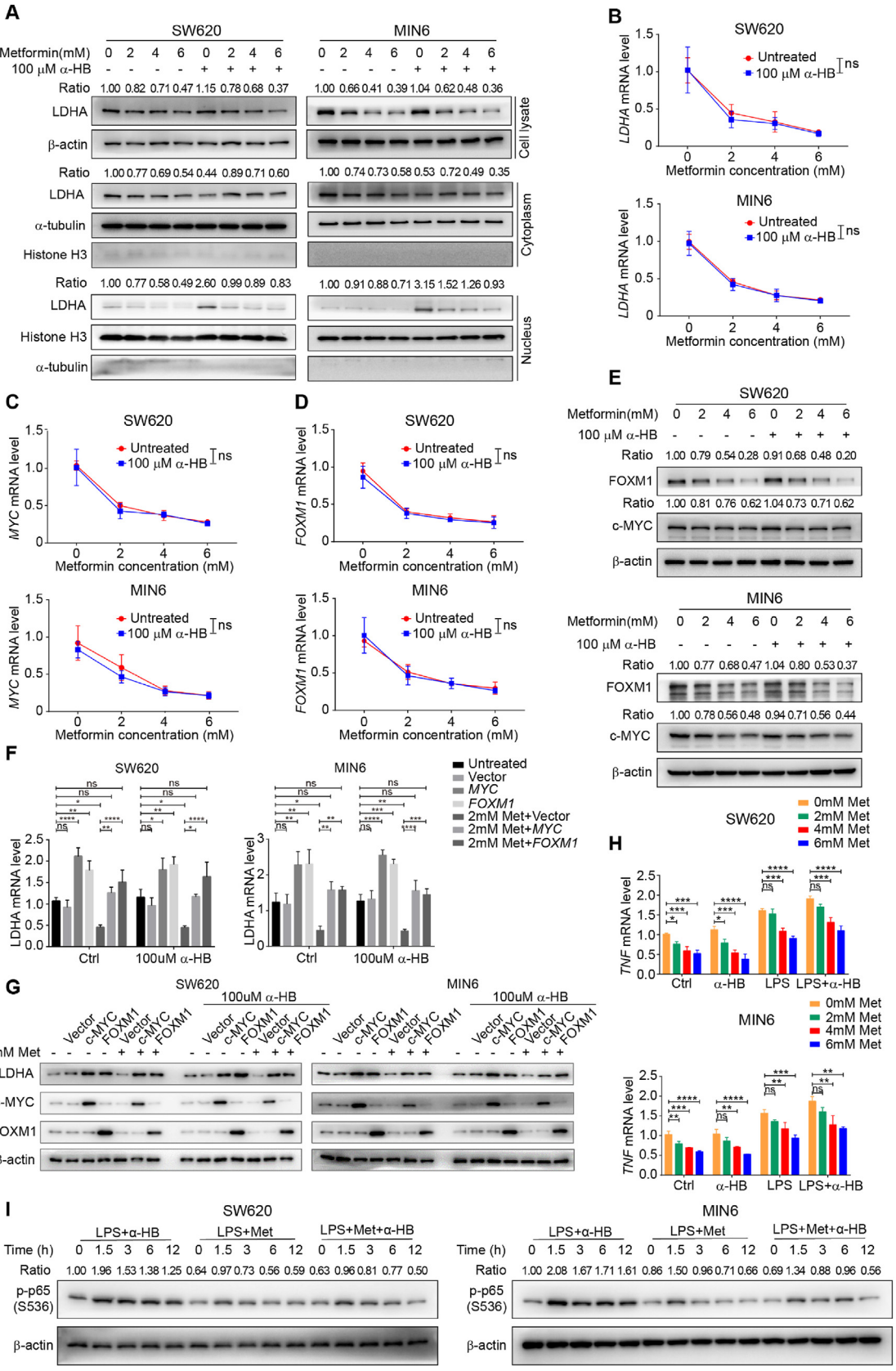

Figure 6: Metformin inhibits NF-κB nuclear retention induced by α-HB. (A) LDHA expression (upper) and cellular distribution in cytoplasmic (middle) and nuclear (bottom) extracts of SW620 and MIN6 cells treated with metformin at different concentrations for 48 h with or without α-HB preincubation. (B) *LDHA* levels in SW620 and MIN6 cells treated with metformin at different concentrations for 36 h with or without α-HB preincubation were determined by RT-PCR. (C–D) *MYC* (C) and *FOXM1* (D) levels in SW620 and MIN6 cells

2.4. α-HB promotes LDHA nuclear translocation to retain nuclear NF-κB

LDHA catalyzes the formation of α-HB from α-KB and may translocate into the nucleus under stressful conditions [13,42]; thus, we explored whether LDHA was involved in α-HB-mediated NF-κB retention.

Although LDHA is typically located in the cytosol, nuclear localization was substantially observed in various cancers, such as CRC, hepatocellular carcinoma, breast cancer, pancreatic cancer, ovarian cancer, gastric cancer, lung cancer, esophageal cancer and lymphoma (Fig. S7A). In addition, LDHA nuclear localization was also observed in all experimental samples of colorectal tissues from α-HB- and/or AOM/DSS-treated mice (Fig. S6D) and in liver (Fig. S6E) and adipose tissues (Fig. S6) from α-HB- and/or HFD-treated mice but not negative control mice. Considering the non-canonical enzyme activity of LDHA to produce α-HB, with higher activity of the nuclear LDHA than cytosolic LDHA [42], the exogenous α-HB may further induce the production of endogenous α-HB by inducing LDHA nuclear translocation in a positive feedback manner (Figures 1J and 2F). The observed nuclear translocation of LDHA in cancer and T2D may result from local oxidative stress, such as ROS. Considering that H_2O_2 could induce LDHA nuclear translocation in cervical cancer [42] and that ROS are commonly produced in cancer [49] and T2D [50], we treated SW620 cells with α-HB or H_2O_2 to mimic in vivo conditions. Either α-HB or H_2O_2 could induce LDHA nuclear translocation, which was further enhanced by combined treatment (Fig. S7B), probably due to a feedback loop in which nuclear LDHA induced by H_2O_2 can further generate α-HB from α-KB [42], which may further potentiate the production of α-HB in the α-HB combined with A/D (Figure 1J) or HFD (Figure 2F) groups. This effect of α-HB on inducing LDHA nuclear translocation was also observed in a dose-dependent manner (Figure 5A and Fig. S7C). Thus, α-HB directly or oxidative stress indirectly promotes LDHA nuclear translocation by producing more α-HB.

Next, we used immunocytochemistry (ICC) assays to identify the subcellular localization and possible interaction of LDHA and NF-κB. LDHA and the NF-κB units p65 and p50 are located in the cytoplasm, and a minority of LDHA and p65 or p50 were further found to colocalize in the absence of α-HB or LPS (top panel in Figure 5B,C). At 1.5 h (Figure 5B) and 12 h (Figure 5C) after α-HB treatment alone, LDHA translocated into the nucleus, while p65 and p50 remained in the cytosol (second panel in Figure 5B,C). In contrast, LPS alone induced the nuclear translocation of p65/p50 but not LDHA at 1.5 h, as expected (third panel in Figure 5B), while at 12 h, p65/p50 was already exported from the nucleus (third panel in Figure 5C). Furthermore, the combined α-HB and LPS treatment induced the nuclear translocation and colocalization of LDHA and p65/p50 at 1.5 h after treatment (bottom panel in Figure 5B); more interestingly, at 12 h, p65/p50 was retained in the nucleus and colocalized with LDHA (bottom panel in Figure 5C). Using immunoblotting, we further found that after persistent α-HB treatment, LDHA accumulated in the nucleus in a time-dependent manner, and LPS had no effect on LDHA nuclear translocation (Figure 5D and Fig. S7D). Interestingly, a single α-HB treatment for 48 h retained LDHA in the nucleus during the 36 days that we tested (Figure 5E). Therefore, these findings indicate that α-HB-induced LDHA nuclear translocation potently prolonged the retention of LPS-induced p65/p50 in the nucleus, most likely via LDHA and NF-κB interactions.

Using a coimmunoprecipitation (Co-IP) assay, we further confirmed that LDHA could interact with p65 and p50, and this effect was markedly strengthened by combined α-HB and LPS treatment (Figure 5F). Notably, α-HB or LPS treatment alone attenuated the interaction (Figure 5F), which was attributed to subcellular spatial separation (Figure 5B). This result suggests that LDHA may bind to the phosphorylated NF-κB induced by LPS. Indeed, after we individually or simultaneously mutated the two LPS-induced phosphorylation sites serine 276 and 536 of p65[51], the interaction between LDHA and NF-κB was obviously weakened by the single-site mutants (S276A or S536A) and completely abrogated by the two-site mutant (S276A and S536A) (Figure 5G). Taken together, these results suggested that after α-HB- and LPS-induced nuclear translocation of LDHA and p65/p50, respectively, LDHA strongly prolonged NF-κB nuclear retention and robustly potentiated NF-κB activation by binding to LPS-activated phosphorylated p65.

2.5. Metformin treatment inhibits nuclear LDHA-induced NF-κB nuclear retention and AOM/DSS-induced CRC

Metformin has been widely recognized as a successful first-line therapy for T2D patients and is further appreciated due to its anti-tumor activity in some diabetic conditions or nondiabetic cancers, especially pancreatic, colorectal and hepatocellular cancers [52,53]. The glucose-lowering effect of metformin is attributed to the inhibition of hepatic gluconeogenesis mainly by targeting AMPK [54], while the antitumor activity of metformin may involve a complicated process with AMPK-dependent and AMPK-independent mechanisms [55]. However, the underlying mechanisms remain elusive. Thus, the versatile functions of metformin prompted us to examine whether metformin was effective in preventing α-HB-prolonged NF-κB activation.

It has been reported that metformin can decrease LDHA via an unknown mechanism [56]; thus, we first examined the effect of metformin on LDHA expression. Metformin decreased LDHA expression regardless of the presence or absence of α-HB treatment, thus reducing LDHA levels in the cytoplasm and nucleus (Figure 6A and Fig. S8A). This effect of metformin on reducing LDHA expression most likely resulted from a decline in LDHA transcription (Figure 6B and Fig. S8B). In addition, we observed that metformin could potently inhibit the nuclear translocation of LDHA induced by α-HB, which was determined by the increased level of cytoplasmic LDHA (middle panel in Figure 6A and Fig. S8A). Furthermore, *FOXM1* and *MYC*, two transcription factors that regulate LDHA expression [57], also showed similar reduction patterns independent of α-HB (Figure 6C—E and Figs. S8C—D), while ectopic expression of FOXM1 or MYC could rescue the expression LDHA decreased by metformin unrelated to α-HB (Figure 6F—G and Figs. S8E—F), suggesting that metformin can suppress LDHA expression at the transcriptional level. Subsequently, metformin reduced LPS- and/or α-HB-induced and NF-κB-mediated

treated with metformin at different concentrations for 30 h with or without α-HB preincubation were determined by RT-PCR. (E) c-MYC and FOXM1 levels in SW620 and MIN6 cells treated with metformin at different concentrations for 36 h with or without α-HB preincubation. (F—G) LDHA levels in SW620 and MIN6 treated with 2 mM Metformin for 48 h with or without α-HB preincubation, along with C-MYC or FOXM1 overexpression were detected by QPCR (F) and Western blot (G). (H) T*NF* levels in SW620 and MIN6 cells treated with LPS for 9 h in the presence or absence of α-HB or preincubated with different concentrations of metformin were determined by RT-PCR. (I) p65 S536 phosphorylation levels in SW620 and MIN6 cells treated with LPS for 1.5 h in the presence or absence of α-HB or incubated with metformin for 48 h. The data are shown as the mean ± SD; Met, metformin; NC, negative control; NS, not significant. Statistical differences were determined by two-way ANOVA test (B—E) and one-way ANOVA test (F, H) with Tukey's multiple comparison with Tukey's multiple comparison. The *p* values were considered significant if < 0.05. *, **, *** and **** denote $p < 0.05$, $p < 0.01$, $p < 0.005$ and $p < 0.001$, respectively.

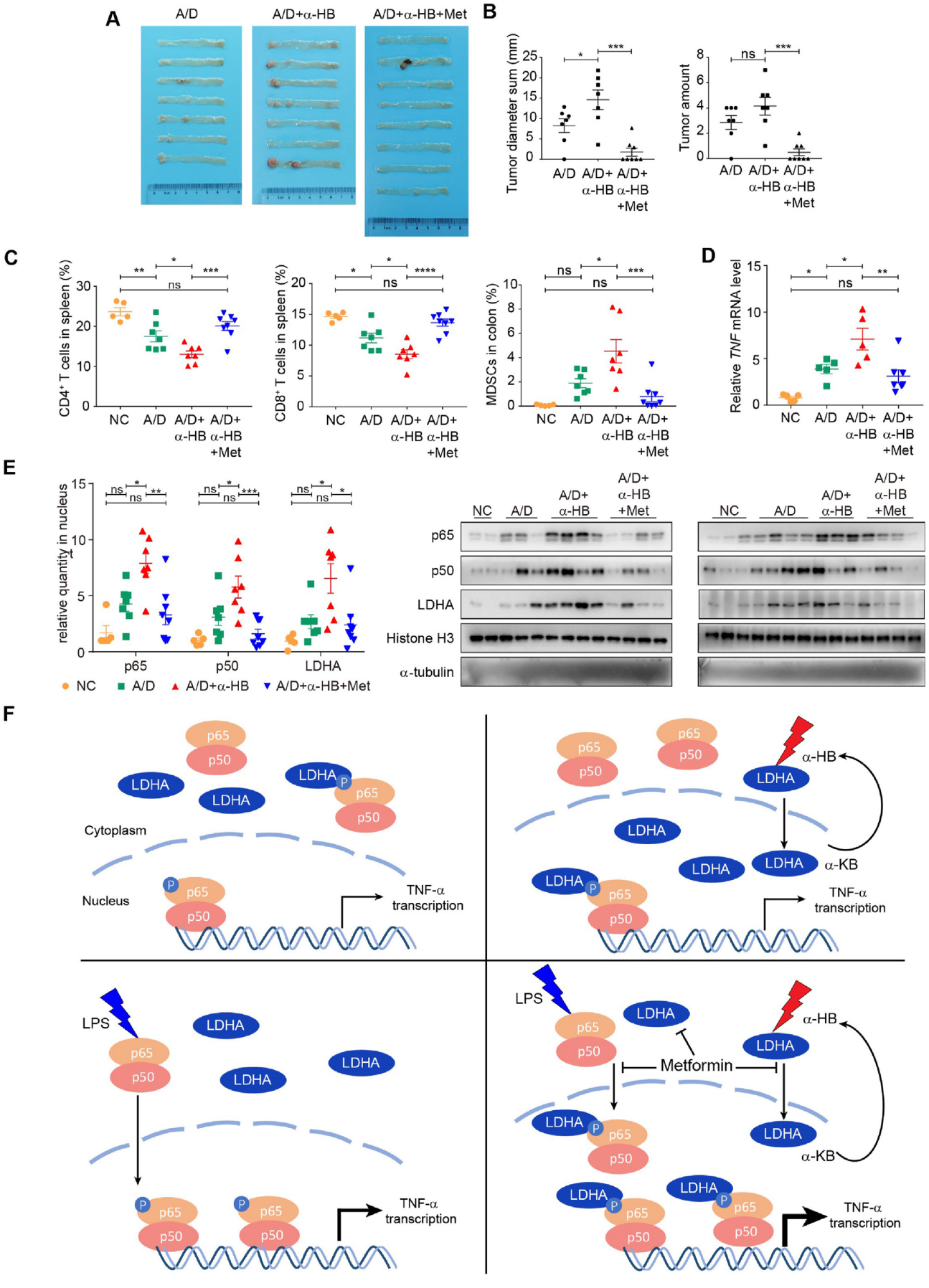

TNF-α production (Figure 6H and Fig. S8G) by suppressing the expression of LDHA (Figure 6A) and thus the activation of NF-κB (Figure 6I and Fig. S8H). Based on these findings, we proposed that metformin could inhibit the α-HB- accelerated development of AOM/DSS-induced CRC and HFD-induced diabetes.

Considering that the effect of metformin on diabetes control has been extensively studied [58], we mainly focused on the effect of metformin on CRC carcinogenesis induced by AOM/DSS and α-HB. In addition to numerous meta-analyses [59] and clinical trials [60], a series of successful in vivo mouse models via AOM/DSS [61], DMH/DSS [62] or DMH [63] with metformin treatment showed metformin could inhibit the development of CRC at various stages. Thus, we further focused on understanding the role of metformin in mitigating the tumorigenic effect of α-HB-enhanced CRC. As shown in Figure 7A,B, combined α-HB treatment increased the tumor size and number induced by AOM/DSS, while metformin administration remarkably protected against α-HB- and AOM/DSS-induced CRC. Again, we observed significantly reduced levels of $CD4^+$ and $CD8^+$ T cells in the spleen and elevated levels of MDSCs in the colon in the AOM/DSS alone group, which was exacerbated by combined α-HB treatment (Figure 7C). However, this trend was reversed by the addition of metformin to a degree similar to that of the negative control group (Figure 7C). Local TNF-α expression exhibited a similar pattern except that metformin treatment failed to reduce TNF-α expression to a level comparable to that of the negative control (Figure 7D), indicating that other mechanisms of TNF-α regulation may be involved in α-HB- and AOM/DSS-induced CRC carcinogenesis. In addition, nuclear levels of NF-κB and LDHA in colorectal sites were also consistent with tumor growth and changes of immune cells. Compared to the negative control, AOM/DSS treatment significantly prompted the nuclear accumulation of p65/p50 and LDHA, while α-HB combined treatment further enhanced the nuclear accumulation, which was effectively inhibited by additional metformin treatment (Figure 7E). These findings suggest that metformin holds potential as an efficient protective drug for α-HB-enhanced CRC.

2.6. Discussion and conclusions

The incidences of glucose dysregulation and cancer are rapidly growing, and epidemiologic evidence has shown a close relationship between them. It has been reported that certain kinds of cancer and diabetes are becoming increasing associated [3], and α-HB, a metabolic byproduct, is usually upregulated in diabetes [24—26] or various cancers [18,20—23]. Here, we revealed that α-HB promoted the development of murine AOM/DSS-induced CRC and HFD-induced diabetes by potentiating NF-κB signaling and provided a novel mechanism by which metformin treats diabetes and cancer. Mechanistically, LDHA can translocate into the nucleus upon α-HB stimulation and then interact with nuclear NF-κB by binding to the phosphorylation sites of p65 induced by activators such as LPS, thus leading to the persistent retention and activation of NF-κB in the nucleus, as represented by elevated TNF-α expression (Fig. 7F). Metformin treatment inhibited the transcription of *FOXM1* and *c-MYC*, transcription factors of LDHA, thus restraining NF-κB activation mediated by α-HB (Fig. 7F).

α-HB is a metabolite produced in methionine-to-glutathione metabolism catalyzed by LDH from α-KB. Due to the abnormal increase in circulating α-HB in insulin resistance [13], and various types of cancers, including CRC [18,19], α-HB has been recommended as a potential screening marker for these disorders. Consistently, we also determined the upregulation of plasma α-HB in the mice administered AOM/DSS or fed a HFD. The accumulation of α-HB may result from increased glutathione synthesis or from the nuclear translocation of LDHA induced by oxidative stress, including ROS [42] and elevated $NADH/NAD^+$ ratios [64], both of which are commonly engaged in the development of cancer and diabetes; however, the underlying mechanism of α-HB in the pathogenesis of these conditions remains obscure [13]. Here, we discovered that α-HB treatment induced LDHA nuclear translocation in colorectal cancer cells and pancreatic β cells. Nuclear LDHA may generate a positive feedback loop by producing more α-HB, which further induces more LDHA nuclear translocation. N-acetylcysteine (NAC), a ROS scavenger, could remarkably reduce LDHA nuclear translocation [42], indicating that anti-inflammation via ROS suppression may decrease α-HB production. Consequently, we observed that with a single administration of α-HB, LDHA can persist in the nucleus for up to 36 days. Furthermore, we and others [21—23] found that nuclear α-HB has also been observed in clinical specimens of a variety of cancers. However, we observed that LDHA nuclear translocation occurred only in some but not all α-HB-treated cells or tumor cells in clinical specimens, and the underlying mechanisms need further investigation. Overall, these findings highlight the importance of investigating the role of α-HB in insulin resistance and cancer.

LDHA is located mainly in the cytosol and catalyzes the conversion of pyruvate to lactate and back; LDHA is also in the nucleus, where it has distinct functions [65]. It has been reported that nuclear LDHA is involved in gene transcription through maintaining the proper NAD^+/NADH ratio [64], epigenetic modifications through DOT1L-induced H3K79 hypermethylation and α-HB production under oxidative stress [42]. Here, we uncovered that α-HB stimulation triggered LDHA nuclear translocation, and then nuclear LDHA bound to LPS-activated nuclear NF-κB at the p65 phosphorylation site, thus markedly extending NF-κB nuclear retention and leading to persistent NF-κB activation. The inflammatory state promotes and often precedes the onset and development of diabetes and a range of cancers, and NF-κB is a key coordinator of these processes [46]. Upon activation, nuclear NF-κB initiates the transcription of multiple proinflammatory factors and cytokines, as represented by TNF-α, a master switch involved in immunity, apoptosis, survival and inflammation. However, nuclear NF-κB is quickly exported to the cytoplasm mainly by the nuclear export sequence (NES) present on IκBα, which shuttles continuously between the nucleus and the cytoplasm [66,67]. However, α-HB treatment markedly extended NF-κB nuclear retention by inducing LDHA nuclear translocation. Nuclear LDHA bound to NF-κB via phosphorylated p65 at

Figure 7: Metformin inhibits α-HB and AOM/DSS-induced murine CRC. (A) Images of colons in the four groups collected at the end of the CRC induction regimen. (B) Tumor diameter sums (left) and numbers (right) were measured and counted. (C) $CD4^+$ T cells (left, defined as $CD3^+$ and $CD4^+$) and $CD8^+$ T cells (middle, defined as $CD3^+$ and $CD8^+$) in the spleen and MDSCs (right, defined as $CD11b^+$ and $Gr\text{-}1^+$) in the colon were determined by flow cytometry. (D) *TNF* levels in the colon were determined by qRT-PCR. (E) Quantification and western blot analysis of p65, p50 and LDHA levels in nuclear extracts of colon tissue in the A/D+α-HB + Met model. Histone H3 was used as a loading control for immunoblotting. (F) Proposed working model showing that nuclear LDHA extends LPS-induced NF-κB nuclear retention. NC, n = 5; A/D, n = 7; A/D+α-HB, n = 7; A/D+α-HB + Met, n = 8. The data are shown as the mean ± SEM. NC, negative control; A/D, AOM/DSS; Met, metformin; NS, not significant. Statistical differences were determined by one-way ANOVA test with Tukey's multiple comparison. The *p* values were considered significant if < 0.05. *, **, *** and **** denote $p < 0.05$, $p < 0.01$, $p < 0.005$ and $p < 0.001$, respectively.

the C-terminal serine 276/536 (S276/536) of p65, and a single site mutation of S276/536 evidently weakened this interaction, while simultaneous mutations in both sites completely abrogated this interaction. Since IκBα also binds to the C-terminus of p65 [68], this interaction of LDHA with phosphorylated p65 may exclude further binding of IκBα to p65 due to steric hindrance, thus resulting in the persistent retention and activation of NF-κB in the nucleus. It should be noted that the effect of α-HB on potentiating NF-κB signaling requiring the pre-activation of NF-κB is applicable to a viariety of cell types including epithelial cells, pancreatic β cells, adipocytes and also likely immune cells. As shown in Figure 1E—G and Figure 2C—D, α-HB alone had no effect on T cells and macrophages, however, the combination of α-HB with other pro-inflammatory stimuli such as DSS and HFD reduced or increased the the proportions of $CD4^+$/$CD8^+$ T cells and MDSCs, respectively in AOM/DSS model, or promoted the M1 polarization of macrophages in HFD-induced T2D model.

Metformin, which is extensively used as a first-line therapy for patients with T2D, also has potential anticancer activity, although the mechanisms have not been fully elucidated. Here, we provide another mechanism by which metformin can treat T2D and cancer. Consistent with previous reports [69—71], we also found that metformin could reduce LDHA expression and further revealed the underlying mechanism by which metformin could downregulate the expression of FOXM1 and c-MYC, two transcription factors of LDHA.

It should be noted that LDHA only binds to phosphorylated p65; therefore, preactivation or nuclear localization of NF-κB is a prerequisite for the deleterious effect of α-HB, in which α-HB potentiates NF-κB activation by inducing LDHA nuclear translocation. Considering that LDHA may persist in the nucleus after α-HB stimulation, our findings reveal the importance of NF-κB inhibitors in preventing α-HB-induced chronic inflammation and resultant disorders, such as T2D and certain types of cancer.

3. METHODS

3.1. Antibodies and reagents

Antibodies against LDHA (Cell Signaling Technology, 3582, 1:300 for ICC and IHC; Santa Cruz, 1:50 working dilution for co-IP; Proteintech, 19987-1-AP, 1:2000 working dilution for western blotting), p65 (Cell Signaling Technology, 8242, 1:1000 working dilution for western blotting, 1:300 for ICC; Cell Signaling Technology, 6956, 1:100 for co-IP), p50 (Cell Signaling Technology, 13,586, 1:1000 working dilution for western blotting, 1:300 for ICC, Santa Cruz, sc-8414, 1: 50 for co-IP), phospho-p65 (Cell Signaling Technology, 3033, 1:1000 working dilution for western blotting), FOXM1 (Proteintech, 13147-1-AP, 1:2000 for western blotting), c-MYC (Proteintech, 10828-1-AP, 1:2000 for western blotting), α-tubulin (Proteintech, HRP-66031, 1:10,000 working dilution for western blotting), Histone H3 (Cell Signaling Technology, 4499, 1:1000 working dilution for western blotting), Lamin B (Santa Cruz, sc-6217, 1:500 working dilution for western blotting), β-actin (Santa Cruz, sc-47778, 1:500 working dilution for western blotting), HA (MBL, 1:100 working dilution for western blotting), CD4 (Abcam, ab183685, 1:1000 working dilution for IHC), and CD8 (Abcam, ab217344, 1:1000 working dilution for IHC) were purchased commercially.

Azoxymethane (Sigma, A5486), dextran sulfate sodium (MP Biomedicals, 9011-18-1), sodium 2-hydroxybutyrate (TCI, H0387), high-fat diet (Research Diets, D12492), metformin (Sigma, D150959), LPS (Beyotime, S1732), DAPI (Yeasen, 36308ES11), PDTC (Selleck, S3633), D-(+)-glucose (Sigma, G7021), IBMX (Santa Cruz, 28,822-58-4), Dexamethasone (Solarbio, D8040) and insulin (Novo Nordisk, Actrapid) were purchased commercially.

3.2. Plasmid construction, site-directed mutagenesis, and transfection

The CDSs of human *p65*, *FOXM1*, and *MYC* genes were amplified with specific PCR primers and subsequently inserted ininserted into pCMV-C-HA to establish plasmids. pCMV-*p65-S276 A/S536 A/S276A + S536A*-C-HA plasmids were further established via site-directed mutagenesis kit (TOYOBO, SMK-101) using specifically designed primers. All plasmids constructs were confirmed by sequencing and then transfected into SW620 or MIN6 cells using Lipofectamine 3000 (Thermo Fisher Scientific, L3000150), as indicated.

3.3. Cell culture

All cell lines were purchased from the Type Culture Collection Cell Bank, Chinese Academy of Sciences. SW620 cells were cultured in L-15 medium (HyClone) supplemented with 10% fetal bovine serum (Gibco) in the presence of penicillin and streptomycin. MIN6 cells were cultured in Roswell Park Memorial Institute (RPMI) 1640 (HyClone) supplemented with 10% fetal bovine serum (Gibco), 50 μM β-mercaptoethanol, and 10 mM HEPES in the presence of penicillin and streptomycin. Cells were cultured at 37 °C in a humidified 5% CO_2 atmosphere. 3T3-L1 cells were cultured in Dulbecco's Modified Eagle Medium (Hyclone) supplemented with 10% bovine calf serum (Gibco) in the presence of penicillin and streptomycin. For adipoctyes differentiation, 3T3-L1 cells were seeded in 12-well plates and cultured until two days after cells reached confluence. Media was refreshed supplemented with 0.5 mM IBMX, 1 μM dexamethasone and 10 μg/mL insulin (day 0). On day 4, media was refreshed supplemented with 10 μg/mL insulin. On day 8, media was refreshed with DMEM with bovine calf serum only. On day 10, fully differentiated adipocyte-like cells should be obtained.

3.4. Animals

Male C57BL/6 mice were purchased from SLAC Laboratory Animal Co., Ltd. (Shanghai, China). The animals were housed in specific pathogen-free conditions with a 12-h light/dark cycle and given free access to food and water. Animal care and experiments were performed with the consent of the Animal Ethics Committee at Shanghai Medical School, Fudan University, and complied with the Guide for the Care and Use of Laboratory Animals published by the US National Institutes of Health.

3.5. Animal models

3.5.1. AOM/DSS-induced CRC model

Mice (6—8 weeks, male) were injected intraperitoneally with 8.5 and 9 mg/kg azoxymethane (AOM, Sigma) on day 1 and 8, respectively. Seven days later, the mice received drinking water containing 2.0% dextran sulfate sodium (DSS) for one week and regular drinking water for 2 weeks, followed by two additional DSS cycles. α-HB (2.0%) was dissolved in drinking water starting at the first DSS cycle.

3.5.2. HFD-induced type 2 diabetes model

Mice were fed a HFD consisting of 60% calories from fat starting at 6 weeks of age for a total of 24 weeks. α-HB (2.0%) was dissolved in drinking water and administered concurrently with HFD feeding.

3.5.3. Metformin treatment in AOM/DSS-induced CRC model

Mice (6—8 weeks, male) were injected intraperitoneally with 8.5 and 9 mg/kg azoxymethane (AOM) on day 1 and 8, respectively. Seven days later, the mice received drinking water containing 2.0% dextran sulfate sodium (DSS) for one week and regular drinking water for 2 weeks, followed by two additional DSS cycles. α-HB (2.0%) and 500 mg/L metformin were dissolved in drinking water starting at the first DSS cycle.

3.5.4. Glucose and insulin tolerance tests

For the glucose tolerance test, we fasted the mice for 16 h, measured blood glucose concentrations, administered an intraperitoneal injection of glucose (1 g/kg body weight) and measured blood glucose concentrations at 15, 30, 60, 90 and 120 min.

For the insulin tolerance test, we fasted the mice for 2 h, measured blood glucose concentrations, administered an intraperitoneal injection of insulin (0.9 units/kg body weight) and measured blood glucose concentrations at 15, 30, 60 and 90 min.

3.6. Tissue sampling, cell separation and flow cytometry

Cells were isolated from different tissues (blood, spleen, colon, liver and epididymal white adipose tissue (EWAT)) for flow cytometry. In brief, blood was collected in an EDTA anticoagulation tube and centrifuged at 2000 rpm/min for 15 min to extract plasma. Red blood cell (RBC) lysis buffer (BioLegend, 420,301) was added to the precipitate to remove erythrocytes, followed by 5 min of centrifugation at 500*g* and a PBS wash. The spleen was ground with PBS and filtered through 300 mesh gauze. Then, the separated cells were collected by 5 min of centrifugation at 500*g*, RBCs were lysed, and splenic cells were washed with PBS. Colon tissue, liver tissue and EWAT were mechanically disrupted in DMEM containing different enzymes, further digested for 15 min with shaking at 37 °C and filtered through 300 mesh gauze. Then, the separated cells were collected by 5 min of centrifugation at 500*g* and washed with PBS.

For cell surface antigen staining, the separated cells were incubated in 1% BSA/PBS containing blocking antibodies for 30 min on ice, followed by 5 min of centrifugation at 1,000 g, after which the cells were suspended in 1% BSA/PBS containing the indicated antibodies and incubated for 1 h on ice. For intracellular staining, cell surface antigen staining was performed first. Then, the cells were fixed in fixation buffer (BioLegend, 420,801) for 30 min, centrifuged at 1,500 g for 5 min, resuspended in intracellular staining perm wash buffer (BioLegend, 421,002) and washed three times, followed by intracellular staining. Samples were measured on a BD FACSCanto II (Beckman Coulter) and analyzed with FlowJo software (Tree Star, Ashland Or). See Table S1 for detailed information on enzymes/antibodies.

3.7. Multiplex assay

Appropriate colon samples were mechanically disrupted in tissue extraction reagent (Thermo Fisher Scientific, 78,510) containing protease and phosphatase inhibitors (Bimake, B14001, B15001), followed by homogenization in a low-temperature grinder. The homogenate was lysed on ice for 2 h and centrifuged at 12,000 g for 10 min to extract colon tissue homogenates (CTHs). CTHs were quantified by a BCA protein quantification kit (Yeasen, 20201ES76) according to the manufacturer's instructions. Then, 50 μg of CTH was subjected to multiplex assays, according to the modified protocols from the manufacturer (Biolegend, 740,005, 740,007, 740,134). Samples were examined on a BD FACS Canto II (Beckman Coulter, Inc., Brea CA) and analyzed with LEGENDplex software (Biolegend).

3.8. Measurement of α-HB concentrations in mouse plasma

3.8.1. α-HB standard curve construction

One milliliter of C57BL/6 mouse EDTA plasma was vigorously mixed with 5 mL of methanol. Following centrifugation, the supernatant was removed and used as the diluent for the α-HB standard. Six concentrations of α-hydroxybutyrate calibrators, 0, 10, 25, 50, 75, and 100 μM, were prepared with the diluent. Linear regression of the peak areas of the α-hydroxybutyrate calibrators against the interval standards was used to determine the standard curve.

3.8.2. Metabolite analysis by LC-MS/MS

Fifty microliters of mouse EDTA plasma was precipitated by being vigorously mixed with 250 μL of methanol. After centrifugation and dilute, 2 μL of the clear sample supernatant was injected and analyzed by multiple reaction monitoring (MRM) via a combination of 6500 Q-Trap triple quadrupole mass spectrometry (AB Sciex) and a Prominence HPLC System (Shimadzu). LC/MS—MS was performed as previously described with replacement of the 1.7 μm Ultimate AQ-C18 column with a 5 μm column.

3.9. Quantitative RT-PCR

Total RNA was isolated from cultured cells or mouse tissue using NucleoZol reagent (Macherey—Nagel, 740404.200) and reverse transcribed according to the manufacturer's instructions (TaKaRa, RR036Q). Then, real-time PCR analysis was performed using SYBR green (TaKaRa, RR820A), and the results were normalized to β-actin in ABI Quant Studio 7. Gene-specific primer sequences are provided in Table S2.

3.10. Coimmunoprecipitation and western blotting

SW620 cells were preincubated with α-HB for 24 h and further stimulated with LPS for 1.5 h. The cells were washed with PBS, collected and lysed for 2 h in ice-cold cell lysis buffer for western blotting and IP (Beyotime, P0013) containing protease and phosphatase inhibitors (Bimake, B14001, B15001). The quantified whole-cell lysates were incubated with antibodies or IgG overnight at 4 °C. Then, 20 μl of protein A/G beads (Bimake, B23202) were added to the lysates and incubated at 4 °C for 4 h. The beads were washed with cell lysis buffer three times and suspended in 45 μl of cell lysis buffer, after which 15 μl of 4 × loading buffer was added and heated at 100 °C for 10 min. Afterwards, western blotting with the indicated antibodies was performed according to standard western blotting protocols.

3.11. Immunocytochemistry

SW620 cells were plated at 1×10^4 per well on glass coverslips in 24-well culture plates and incubated with 100 μM α-HB and/or 5 ng/mL LPS for the indicated times. Cells were fixed with 4% paraformaldehyde for 15 min at room temperature and washed three times with PBS. Cells were then permeabilized with 0.2% Triton-X-100 in 1% BSA/PBS for 5 min at 4 °C and washed three times with PBS. Blocking was performed with 1% BSA/PBS for 1 h at room temperature, followed by primary antibody incubation in blocking buffer overnight at 4 °C. Then, the cells were washed three times and incubated with the indicated secondary antibody in blocking buffer for 2 h at room temperature. After three washes, DAPI was added, and the samples were stored at 4 °C.

3.12. Immunohistochemistry

Human tumor samples were acquired from Fudan University Shanghai Cancer Center. Informed consent was obtained from each patient. The

human studies were approved by the Ethics Committee of Fudan University Shanghai Cancer Center, Shanghai, China, and performed in compliance with the relevant ethical regulations.

Approximately 1–2-cm of mouse colon segments or human tumor samples were fixed in 4% paraformaldehyde overnight, embedded in paraffin blocks, and cut into 5 cm sections. The sections were deparaffinized and rehydrated before being subjected to high-pressure antigen retrieval in citrate buffer (pH 6.0), followed by endogenous peroxidase blocking with 3% hydrogen peroxide at 37 °C for 15 min. After being rinsed with PBS, the sections were blocked with goat serum in 1% BSA/PBS for cell surface staining or with 0.3% Triton-x-100 for intracellular staining at room temperature for 1 h and incubated with primary antibodies at 4 °C overnight. After being rinsed with PBS, HRP-conjugated secondary antibodies were added and incubated at room temperature for 1 h. Then, DAB reactions were performed by a GTVision III immunohistochemical detection kit (Gene Tech, GK500705) according to the manufacturer's instructions.

3.13. Cytoplasmic and nuclear extraction

Isolation of cytoplasm and nuclei from cells or tissue samples was performed using a nuclear extract kit (Active Motif, 40,010). In brief, samples were collected and lysed with hypotonic buffer for 15 min at 4 °C, followed by 1 min of centrifugation at 14,000 g to extract cytoplasm. The precipitate was then resuspended in complete lysis buffer for 30 min at 4 °C, followed by 10 min of centrifugation at 14,000 g to extract nuclei.

3.14. ELISA

3.14.1. TNF-α concentration in SW620 supernatant

SW620 cells were plated at 2×10^5 per well in 24-well culture and incubated with LPS with or without α-HB for 60 h. The culture medium was collected and centrifuged at 12,000 g to extract the supernatants. The level of TNF-α in the supernatants was quantified by using an ELISA kit according to the manufacturer's instructions (R&D, DY210).

3.14.2. TNF-α and IL-6 concentration in CTH

CTH extraction was performed as described above. 50 μg of CTH was subjected to ELISA assays, according to the modified protocols from the manufacturer (Proteintech, KE10002; R&D, DY406).

3.14.3. Glucose-stimulated insulin secretion

MIN6 cells were plated at 5×10^4 per well in 48-well plates and cultured with 100 μM α-HB and/or 10 μM PDTC for 12 h, followed by incubated with 50 ng/mL LPS for another 12 h. Then, the cells were washed twice with Krebs–Ringer bicarbonate HEPES buffer (KRBH) and incubated with 100 μl of KRBH for 0.5 h. After removing the supernatant, the cells were incubated with 100 μl of 3 mM or 30 mM glucose in KRBH with the indicated concentrations of α-HB, LPS and PDTC for 2 h. At the end of the incubation, supernatants were collected, and insulin concentrations were measured using an insulin ELISA kit (Mercodia, 10-1247-01). Cells were then collected for protein quantitation.

3.15. Statistical analysis

We analyzed data from three biological replicates unless indicated other in the figure legends. Statistical analyses were performed with two-tailed unpaired Student's *t*-tests, one-way or two-way analysis of variance or multiple *t*-tests. The *p* values were considered significant if < 0.05. *, **, *** and **** denote $p < 0.05$, $p < 0.01$, $p < 0.005$ and $p < 0.001$, respectively. GraphPad Prism 7 (GraphPad, San Diego, CA) was used to perform all statistical analyses and determine *p*-values.

AUTHOR CONTRIBUTIONS

W.H. conceived and supervised the project; W.H. and X.L. designed the experiments and wrote the manuscript; X.L. performed most of the experiments and analyzed the data, with assistance from P.D., Luying Li, Ling Li, D.Z., X.W., J.C., W.Z., Q.W. and T.L.; QY.L., X.H., QH.J., D.Z. and W.W. contributed ideas.

DECLARATION OF COMPETING INTEREST

The authors declare that they have no conflicts of interest.

DATA AVAILABILITY

Data will be made available on request.

ACKNOWLEDGMENTS

This work was supported by grants to W.H. from the National Natural Science Foundation of China (81790254, 91629301, 81872354 and 82121004) and the Major State Basic Research Development Program of China (2013CB910802).

APPENDIX A. SUPPLEMENTARY DATA

Supplementary data to this article can be found online at https://doi.org/10.1016/j.molmet.2023.101766.

REFERENCES

[1] Sung H, Ferlay J, Siegel RL, Laversanne M, Soerjomataram I, Jemal A, et al. Global cancer statistics 2020: globocan estimates of incidence and mortality worldwide for 36 cancers in 185 countries. CA Cancer J Clin 2021;71(3):209–49. https://doi.org/10.3322/caac.21660.

[2] Lega IC, Lipscombe LL. Review: diabetes, obesity, and cancer-pathophysiology and clinical implications. Endocr Rev 2020;41(1). https://doi.org/10.1210/endrev/bnz014.

[3] Gallagher EJ, LeRoith D. Obesity and diabetes: the increased risk of cancer and cancer-related mortality. Physiol Rev 2015;95(3):727–48. https://doi.org/10.1152/physrev.00030.2014.

[4] Giovannucci E, Harlan DM, Archer MC, Bergenstal RM, Gapstur SM, Habel LA, et al. Diabetes and cancer: a consensus report. Diabetes Care 2010;33(7):1674–85. https://doi.org/10.2337/dc10-0666.

[5] Rani V, Deep G, Singh RK, Palle K, Yadav UC. Oxidative stress and metabolic disorders: pathogenesis and therapeutic strategies. Life Sci 2016;148:183–93. https://doi.org/10.1016/j.lfs.2016.02.002.

[6] Marchi S, Guilbaud E, Tait SWG, Yamazaki T, Galluzzi L. Mitochondrial control of inflammation. Nat Rev Immunol 2023;23(3):159–73. https://doi.org/10.1038/s41577-022-00760-x.

[7] Egger G. In search of a germ theory equivalent for chronic disease. Prev Chronic Dis 2012;9:E95. https://doi.org/10.5888/pcd9.110301.

[8] Taniguchi K, Karin M. NF-kappaB, inflammation, immunity and cancer: coming of age. Nat Rev Immunol 2018;18(5):309–24. https://doi.org/10.1038/nri.2017.142.

[9] Esser N, Legrand-Poels S, Piette J, Scheen AJ, Paquot N. Inflammation as a link between obesity, metabolic syndrome and type 2 diabetes. Diabetes Res Clin Pract 2014;105(2):141–50. https://doi.org/10.1016/j.diabres.2014.04.006.

[10] Hu X, Guo F. Amino acid sensing in metabolic homeostasis and health. Endocr Rev 2021;42(1):56–76. https://doi.org/10.1210/endrev/bnaa026.

[11] Natesan V, Kim SJ. Lipid metabolism, disorders and therapeutic drugs - review. Biomol Ther (Seoul) 2021;29(6):596–604. https://doi.org/10.4062/biomolther.2021.122.

[12] Supabphol S, Seubwai W, Wongkham S, Saengboonmee C. High glucose: an emerging association between diabetes mellitus and cancer progression. J Mol Med (Berl) 2021;99(9):1175–93. https://doi.org/10.1007/s00109-021-02096-w.

[13] Gall WE, Beebe K, Lawton KA, Adam KP, Mitchell MW, Nakhle PJ, et al. Alpha-hydroxybutyrate is an early biomarker of insulin resistance and glucose intolerance in a nondiabetic population. PLoS One 2010;5(5):e10883. https://doi.org/10.1371/journal.pone.0010883.

[14] Wu J, Yeung SJ, Liu S, Qdaisat A, Jiang D, Liu W, et al. Cyst(e)ine in nutrition formulation promotes colon cancer growth and chemoresistance by activating mTORC1 and scavenging ROS. Signal Transduct Target Ther 2021;6(1):188. https://doi.org/10.1038/s41392-021-00581-9.

[15] Ogawa S, Takiguchi J, Shimizu M, Nako K, Okamura M, Kinouchi Y, et al. The relationship between the renal reabsorption of cysteine and the lowered urinary pH in diabetics. Clin Exp Nephrol 2017;21(6):1044–52. https://doi.org/10.1007/s10157-017-1401-1.

[16] Castano-Martinez T, Schumacher F, Schumacher S, Kochlik B, Weber D, Grune T, et al. Methionine restriction prevents onset of type 2 diabetes in NZO mice. FASEB J 2019;33(6):7092–102. https://doi.org/10.1096/fj.201900150R.

[17] Gao X, Sanderson SM, Dai Z, Reid MA, Cooper DE, Lu M, et al. Dietary methionine influences therapy in mouse cancer models and alters human metabolism. Nature 2019;572(7769):397–401. https://doi.org/10.1038/s41586-019-1437-3.

[18] Qiu Y, Cai G, Su M, Chen T, Zheng X, Xu Y, et al. Serum metabolite profiling of human colorectal cancer using GC-TOFMS and UPLC-QTOFMS. J Proteome Res 2009;8(10):4844–50. https://doi.org/10.1021/pr9004162.

[19] Barberini L, Restivo A, Noto A, Deidda S, Fattuoni C, Fanos V, et al. A gas chromatography-mass spectrometry (GC-MS) metabolomic approach in human colorectal cancer (CRC): the emerging role of monosaccharides and amino acids. Ann Transl Med 2019;7(23):727. https://doi.org/10.21037/atm.2019.12.34.

[20] Zeng J, Yin P, Tan Y, Dong L, Hu C, Huang Q, et al. Metabolomics study of hepatocellular carcinoma: discovery and validation of serum potential biomarkers by using capillary electrophoresis-mass spectrometry. J Proteome Res 2014;13(7):3420–31. https://doi.org/10.1021/pr500390y.

[21] Yu L, Aa J, Xu J, Sun M, Qian S, Cheng L, et al. Metabolomic phenotype of gastric cancer and precancerous stages based on gas chromatography time-of-flight mass spectrometry. J Gastroenterol Hepatol 2011;26(8):1290–7. https://doi.org/10.1111/j.1440-1746.2011.06724.x.

[22] Hori S, Nishiumi S, Kobayashi K, Shinohara M, Hatakeyama Y, Kotani Y, et al. A metabolomic approach to lung cancer. Lung Cancer 2011;74(2):284–92. https://doi.org/10.1016/j.lungcan.2011.02.008.

[23] Stenson M, Pedersen A, Hasselblom S, Nilsson-Ehle H, Karlsson BG, Pinto R, et al. Serum nuclear magnetic resonance-based metabolomics and outcome in diffuse large B-cell lymphoma patients - a pilot study. Leuk Lymphoma 2016;57(8):1814–22. https://doi.org/10.3109/10428194.2016.1140164.

[24] Menni C, Fauman E, Erte I, Perry JR, Kastenmuller G, Shin SY, et al. Biomarkers for type 2 diabetes and impaired fasting glucose using a nontargeted metabolomics approach. Diabetes 2013;62(12):4270–6. https://doi.org/10.2337/db13-0570.

[25] Varvel SA, Pottala JV, Thiselton DL, Caffrey R, Dall T, Sasinowski M, et al. Serum alpha-hydroxybutyrate (alpha-HB) predicts elevated 1 h glucose levels and early-phase beta-cell dysfunction during OGTT. BMJ Open Diabetes Res Care 2014;2(1):e000038. https://doi.org/10.1136/bmjdrc-2014-000038.

[26] Cobb J, Eckhart A, Motsinger-Reif A, Carr B, Groop L, Ferrannini E. Alpha-Hydroxybutyric Acid Is a Selective Metabolite Biomarker of Impaired Glucose Tolerance. Diabetes Care 2016;39(6):988–95. https://doi.org/10.2337/dc15-2752.

[27] Shantavasinkul PC, Muehlbauer MJ, Bain JR, Ilkayeva OR, Craig DM, Newgard CB, et al. Improvement in insulin resistance after gastric bypass surgery is correlated with a decline in plasma 2-hydroxybutyric acid. Surg Obes Relat Dis 2018;14(8):1126–32. https://doi.org/10.1016/j.soard.2018.03.033.

[28] Moore SC, Matthews CE, Sampson JN, Stolzenberg-Solomon RZ, Zheng W, Cai Q, et al. Human metabolic correlates of body mass index. Metabolomics 2014;10(2):259–69. https://doi.org/10.1007/s11306-013-0574-1.

[29] Hsu YH, Astley CM, Cole JB, Vedantam S, Mercader JM, Metspalu A, et al. Integrating untargeted metabolomics, genetically informed causal inference, and pathway enrichment to define the obesity metabolome. Int J Obes (Lond) 2020;44(7):1596–606. https://doi.org/10.1038/s41366-020-0603-x.

[30] Laursen MR, Hansen J, Elkjaer C, Stavnager N, Nielsen CB, Pryds K, et al. Untargeted metabolomics reveals a mild impact of remote ischemic conditioning on the plasma metabolome and alpha-hydroxybutyrate as a possible cardioprotective factor and biomarker of tissue ischemia. Metabolomics 2017;13(6):67. https://doi.org/10.1007/s11306-017-1202-2.

[31] Lin Z, Vicente Goncalves CM, Dai L, Lu HM, Huang JH, Ji H, et al. Exploring metabolic syndrome serum profiling based on gas chromatography mass spectrometry and random forest models. Anal Chim Acta 2014;827:22–7. https://doi.org/10.1016/j.aca.2014.04.008.

[32] Neufert C, Becker C, Neurath MF. An inducible mouse model of colon carcinogenesis for the analysis of sporadic and inflammation-driven tumor progression. Nat Protoc 2007;2(8):1998–2004. https://doi.org/10.1038/nprot.2007.279.

[33] Ding P, Li L, Li L, Lv X, Zhou D, Wang Q, et al. C5aR1 is a master regulator in Colorectal Tumorigenesis via Immune modulation. Theranostics 2020;10(19):8619–32. https://doi.org/10.7150/thno.45058.

[34] Han Y, Liu Q, Hou J, Gu Y, Zhang Y, Chen Z, et al. Tumor-induced generation of splenic erythroblast-like ter-cells promotes tumor progression. Cell 2018;173(3):634–648 e612. https://doi.org/10.1016/j.cell.2018.02.061.

[35] Grivennikov S, Karin E, Terzic J, Mucida D, Yu GY, Vallabhapurapu S, et al. IL-6 and Stat3 are required for survival of intestinal epithelial cells and development of colitis-associated cancer. Cancer Cell 2009;15(2):103–13. https://doi.org/10.1016/j.ccr.2009.01.001.

[36] Mukaida N, Sasakki S, Popivanova BK. Tumor necrosis factor (tnf) and chemokines in colitis-associated cancer. Cancers (Basel) 2011;3(3):2811–26. https://doi.org/10.3390/cancers3032811.

[37] Salomon BL, Leclerc M, Tosello J, Ronin E, Piaggio E, Cohen JL. Tumor necrosis factor alpha and regulatory t cells in oncoimmunology. Front Immunol 2018;9:444. https://doi.org/10.3389/fimmu.2018.00444.

[38] Bertrand F, Rochotte J, Colacios C, Montfort A, Tilkin-Mariame AF, Touriol C, et al. Blocking tumor necrosis factor alpha enhances cd8 t-cell-dependent immunity in experimental melanoma. Cancer Res 2015;75(13):2619–28. https://doi.org/10.1158/0008-5472.CAN-14-2524.

[39] Slight SR, Rangel-Moreno J, Gopal R, Lin Y, Fallert Junecko BA, Mehra S, et al. CXCR5(+) T helper cells mediate protective immunity against tuberculosis. J Clin Invest 2013;123(2):712–26. https://doi.org/10.1172/JCI65728.

[40] Saez de Guinoa J, Barrio L, Mellado M, Carrasco YR. CXCL13/CXCR5 signaling enhances BCR-triggered B-cell activation by shaping cell dynamics. Blood 2011;118(6):1560–9. https://doi.org/10.1182/blood-2011-01-332106.

[41] Terzic J, Grivennikov S, Karin E, Karin M. Inflammation and colon cancer. Gastroenterology 2010;138(6):2101–14. https://doi.org/10.1053/j.gastro.2010.01.058. e2105.

[42] Liu Y, Guo JZ, Liu Y, Wang K, Ding W, Wang H, et al. Nuclear lactate dehydrogenase a senses ros to produce alpha-hydroxybutyrate for hpv-induced cervical tumor growth. Nat Commun 2018;9(1):4429. https://doi.org/10.1038/s41467-018-06841-7.

[43] Koufakis T, Dimitriadis G, Metallidis S, Zebekakis P, Kotsa K. The role of autoimmunity in the pathophysiology of type 2 diabetes: looking at the other side of the moon. Obes Rev 2021;22(8):e13231. https://doi.org/10.1111/obr.13231.

[44] Orliaguet L, Dalmas E, Drareni K, Venteclef N, Alzaid F. Mechanisms of macrophage polarization in insulin signaling and sensitivity. Front Endocrinol (Lausanne) 2020;11:62. https://doi.org/10.3389/fendo.2020.00062.

[45] Jayashree B, Bibin YS, Prabhu D, Shanthirani CS, Gokulakrishnan K, Lakshmi BS, et al. Increased circulatory levels of lipopolysaccharide (LPS) and zonulin signify novel biomarkers of proinflammation in patients with type 2 diabetes. Mol Cell Biochem 2014;388(1-2):203—10. https://doi.org/10.1007/s11010-013-1911-4.

[46] Tornatore L, Thotakura AK, Bennett J, Moretti M, Franzoso G. The nuclear factor kappa B signaling pathway: integrating metabolism with inflammation. Trends Cell Biol 2012;22(11):557—66. https://doi.org/10.1016/j.tcb.2012.08.001.

[47] Kong SY, Tran HQ, Gewirtz AT, McKeown-Eyssen G, Fedirko V, Romieu I, et al. Serum endotoxins and flagellin and risk of colorectal cancer in the european prospective investigation into cancer and nutrition (epic) cohort. Cancer Epidemiol Biomarkers Prev 2016;25(2):291—301. https://doi.org/10.1158/1055-9965.EPI-15-0798.

[48] Burke SJ, Stadler K, Lu D, Gleason E, Han A, Donohoe DR, et al. IL-1beta reciprocally regulates chemokine and insulin secretion in pancreatic beta-cells via NF-kappaB. Am J Physiol Endocrinol Metab 2015;309(8):E715—26. https://doi.org/10.1152/ajpendo.00153.2015.

[49] Moloney JN, Cotter TG. ROS signalling in the biology of cancer. Semin Cell Dev Biol 2018;80:50—64. https://doi.org/10.1016/j.semcdb.2017.05.023.

[50] Burgos-Moron E, Abad-Jimenez Z, Maranon AM, Iannantuoni F, Escribano-Lopez I, Lopez-Domenech S, et al. Relationship Between Oxidative Stress, ER Stress, and Inflammation in Type 2 Diabetes: The Battle Continues. J Clin Med 2019;8(9). https://doi.org/10.3390/jcm8091385.

[51] Choi HJ, Eun JS, Park YR, Kim DK, Li R, Moon WS, et al. Ikarisoside A inhibits inducible nitric oxide synthase in lipopolysaccharide-stimulated RAW 264.7 cells via p38 kinase and nuclear factor-kappaB signaling pathways. Eur J Pharmacol 2008;601(1-3):171—8. https://doi.org/10.1016/j.ejphar.2008.09.032.

[52] Pollak M. Metformin and pancreatic cancer: a clue requiring investigation. Clin Cancer Res 2012;18(10):2723—5. https://doi.org/10.1158/1078-0432.CCR-12-0694.

[53] Yu H, Zhong X, Gao P, Shi J, Wu Z, Guo Z, et al. The potential effect of metformin on cancer: an umbrella review. Front Endocrinol (Lausanne) 2019;10:617. https://doi.org/10.3389/fendo.2019.00617.

[54] LaMoia TE, Shulman GI. Cellular and molecular mechanisms of metformin action. Endocr Rev 2021;42(1):77—96. https://doi.org/10.1210/endrev/bnaa023.

[55] Pernicova I, Korbonits M. Metformin–mode of action and clinical implications for diabetes and cancer. Nat Rev Endocrinol 2014;10(3):143—56. https://doi.org/10.1038/nrendo.2013.256.

[56] Wahdan-Alaswad RS, Edgerton SM, Salem HS, Thor AD. Metformin targets glucose metabolism in triple negative breast cancer. J Oncol Transl Res 2018;4(1). https://doi.org/10.4172/2476-2261.1000129.

[57] Augoff K, Hryniewicz-Jankowska A, Tabola R. Lactate dehydrogenase 5: an old friend and a new hope in the war on cancer. Cancer Lett 2015;358(1):1—7. https://doi.org/10.1016/j.canlet.2014.12.035.

[58] Sanchez-Rangel E, Inzucchi SE. Metformin: clinical use in type 2 diabetes. Diabetologia 2017;60(9):1586—93. https://doi.org/10.1007/s00125-017-4336-x.

[59] Coyle C, Cafferty FH, Vale C, Langley RE. Metformin as an adjuvant treatment for cancer: a systematic review and meta-analysis. Ann Oncol 2016;27(12):2184—95. https://doi.org/10.1093/annonc/mdw410.

[60] Higurashi T, Hosono K, Takahashi H, Komiya Y, Umezawa S, Sakai E, et al. Metformin for chemoprevention of metachronous colorectal adenoma or polyps in post-polypectomy patients without diabetes: a multicentre double-blind, placebo-controlled, randomised phase 3 trial. Lancet Oncol 2016;17(4):475—83. https://doi.org/10.1016/S1470-2045(15)00565-3.

[61] Kattar SA, Jurjus R, Pinon A, Leger DY, Jurjus A, Boukarim C, et al. Metformin and probiotics in the crosstalk between colitis-associated colorectal cancer and diabetes in mice. Cancers (Basel) 2020;12(7). https://doi.org/10.3390/cancers12071857.

[62] Li W, Wang QL, Liu X, Dong SH, Li HX, Li CY, et al. Combined use of vitamin D3 and metformin exhibits synergistic chemopreventive effects on colorectal neoplasia in rats and mice. Cancer Prev Res (Phila) 2015;8(2):139—48. https://doi.org/10.1158/1940-6207.CAPR-14-0128.

[63] Bordini HP, Kremer JL, Fagundes TR, Melo GP, Conchon-Costa I, da Silva SS, et al. Protective effect of metformin in an aberrant crypt foci model induced by 1,2-dimethylhydrazine: modulation of oxidative stress and inflammatory process. Mol Carcinog 2017;56(3):913—22. https://doi.org/10.1002/mc.22545.

[64] Dai RP, Yu FX, Goh SR, Chng HW, Tan YL, Fu JL, et al. Histone 2B (H2B) expression is confined to a proper NAD+/NADH redox status. J Biol Chem 2008;283(40):26894—901. https://doi.org/10.1074/jbc.M804307200.

[65] Williams KR, Reddigari S, Patel GL. Identification of a nucleic acid helix-destabilizing protein from rat liver as lactate dehydrogenase-5. Proc Natl Acad Sci U S A 1985;82(16):5260—4. https://doi.org/10.1073/pnas.82.16.5260.

[66] Huang TT, Kudo N, Yoshida M, Miyamoto S. A nuclear export signal in the N-terminal regulatory domain of IkappaBalpha controls cytoplasmic localization of inactive NF-kappaB/IkappaBalpha complexes. Proc Natl Acad Sci U S A 2000;97(3):1014—9. https://doi.org/10.1073/pnas.97.3.1014.

[67] Johnson C, Van Antwerp D, Hope TJ. An N-terminal nuclear export signal is required for the nucleocytoplasmic shuttling of IkappaBalpha. EMBO J 1999;18(23):6682—93. https://doi.org/10.1093/emboj/18.23.6682.

[68] Sue SC, Dyson HJ. Interaction of the IkappaBalpha C-terminal PEST sequence with NF-kappaB: insights into the inhibition of NF-kappaB DNA binding by IkappaBalpha. J Mol Biol 2009;388(4):824—38. https://doi.org/10.1016/j.jmb.2009.03.048.

[69] Figueroa-Gonzalez G, Garcia-Castillo V, Coronel-Hernandez J, Lopez-Urrutia E, Leon-Cabrera S, Arias-Romero LE, et al. Anti-inflammatory and antitumor activity of a triple therapy for a colitis-related colorectal cancer. J Cancer 2016;7(12):1632—44. https://doi.org/10.7150/jca.13123.

[70] Tang D, Xu L, Zhang M, Dorfman RG, Pan Y, Zhou Q, et al. Metformin facilitates BG45induced apoptosis via an antiWarburg effect in cholangiocarcinoma cells. Oncol Rep 2018;39(4):1957—65. https://doi.org/10.3892/or.2018.6275.

[71] Nazer RI, Abalhassan MF, Alburikan KA. Liver enzyme trends in patients taking uninterrupted metformin before and after coronary surgery. Cardiovasc Diagn Ther 2018;8(4):469—79. https://doi.org/10.21037/cdt.2018.05.04.

